NASA TECHNICAL MEMORANDUM

NASA TM X-2973

NASA TM X-2973

FORWARD-SLANTED SLOT THROAT STABILITY BYPASS TO INCREASE THE STABLE AIRFLOW RANGE OF A MACH 2.5 INLET WITH 60-PERCENT INTERNAL CONTRACTION

by Robert J. Shaw, Glenn A. Mitchell, and Bobby W. Sanders

Lewis Research Center
Cleveland, Ohio 44135

NATIONAL AERONAUTICS AND SPACE ADMINISTRATION • WASHINGTON, D. C. • MAY 1974

1. Report No. NASA TM X-2973	2. Government Accession No.	3. Recipient's Catalog No.
4. Title and Subtitle FORWARD-SLANTED SLOT THROAT STABILITY BYPASS TO INCREASE THE STABLE AIRFLOW RANGE OF A MACH 2.5 INLET WITH 60-PERCENT INTERNAL CONTRACTION		5. Report Date May 1974 6. Performing Organization Code
7. Author(s) Robert J. Shaw, Glenn A. Mitchell, and Bobby W. Sanders		8. Performing Organization Report No. E-7706 10. Work Unit No. 501-24
9. Performing Organization Name and Address Lewis Research Center, National Aeronautics and Space Administration, Cleveland, Ohio 44135		11. Contract or Grant No. 13. Type of Report and Period Covered Technical Memorandum
12. Sponsoring Agency Name and Address National Aeronautics and Space Administration, Washington, D.C. 20546		14. Sponsoring Agency Code

15. Supplementary Notes

16. Abstract

The results of an experimental investigation to increase the stable airflow operating range of a supersonic mixed-compression inlet are presented. Two forward-slanted slot stability-bypass entrance configurations were tested. In terms of diffuser-exit corrected airflow, a large inlet stable airflow range of 18.5 percent was obtained with the superior configuration if a constant pressure was maintained in the bypass plenum. Limited unstart angle-of-attack data are presented.

17. Key Words (Suggested by Author(s))

Air intakes; Supersonic cruise inlets; Shock stability; Inlet bleed; Throat-bypass bleed; Throat stability bypass

18. Distribution Statement

Unclassified - unlimited
Category 01

19. Security Classif. (of this report)	20. Security Classif. (of this page)	21. No. of Pages	22. Price*
Unclassified	Unclassified	48	$3.25

* For sale by the National Technical Information Service, Springfield, Virginia 22151

FORWARD-SLANTED SLOT THROAT STABILITY BYPASS TO INCREASE THE STABLE AIRFLOW RANGE OF A MACH 2.5 INLET WITH 60-PERCENT INTERNAL CONTRACTION

by Robert J. Shaw, Glenn A. Mitchell, and Bobby W. Sanders

Lewis Research Center

SUMMARY

An experimental investigation was conducted to evaluate the effectiveness of two forward-slanted slot, throat stability-bypass entrance configurations in providing an increased inlet stable airflow operating range. The inlet used for this study was an axisymmetric, mixed-compression type with 60 percent of the supersonic area contraction occurring internally at the design Mach number of 2.50.

Depending on the amount of initial total forward cowl bleed and stability-bypass mass flow, both forward slanted slot configurations provided the inlet with large stability ranges when operating at high-performance conditions. In terms of diffuser-exit corrected airflow, the superior inlet configuration could accept an 18.5-percent reduction before unstart if a constant pressure was maintained in the bypass plenum. Both forward slanted slot configurations incurred a separation of the bypass flow entering the slot passage, which adversely affected stability performance at the higher bypass flows.

With no stability-bypass flow, both inlet configurations exhibited angle-of-attack tolerances that were commensurate with the results of previous tests on the same inlet model with only performance bleed capabilities. Angle-of-attack unstarts were caused by an overcompression of the diffuser flow field on the leeward side and resulting local flow choking.

INTRODUCTION

At flight speeds above Mach 2.0 an inlet having a mixture of internal and external compression offers high performance by supplying the engine with airflow at a high-pressure level while maintaining low drag. To provide optimum internal performance for this type of inlet, the terminal shock must be kept at the inlet throat. However,

mixed-compression inlets suffer from an undesirable airflow characteristic known as unstart. The closer the terminal shock to the throat, the smaller the disturbance that will cause an unstart. This airflow disturbance causes the terminal shock to move forward of the throat where it is unstable and is violently expelled ahead of the inlet cowling. This shock expulsion or unstart causes a large rapid variation in mass flow and pressure recovery and, thus, a large thrust loss and drag increase. Inlet buzz, compressor stall, and/or combustor blowout may also occur. Obviously, an inlet unstart is extremely undesirable, not only because of the effects on the propulsion system itself, but also on the aerodynamic qualities of the aircraft. If an inlet unstart does occur, large variations of the inlet geometry are required to reestablish initial design operating conditions.

Both external airflow transients such as atmospheric turbulence and internal airflow changes such as a reduction in engine airflow demand can cause the inlet to unstart. It is desirable for the inlet to have a large enough stable margin to absorb such transients without unstarting. For an internal airflow change the inlet should provide a margin in corrected airflow below the value for optimum performance without incurring unstart. This margin is defined as the stable airflow operating range. Conventional mixed compression inlets can be designed to have some stable range provided by the capacity of the performance-bleed systems. Since performance-bleed exit areas are generally fixed, this stable range may not be adequate to absorb many of the airflow transients that are encountered by a typical supersonic propulsion system. An increased stable range may be provided by operating supercritically with a resultant loss in performance. Since any loss in performance is reflected directly as a loss in thrust, supercritical operation should be avoided.

To provide the necessary stable operating range without compromising steady-state performance, the inlet can be designed to replace the throat bleed with a throat stability-bypass system capable of removing large amounts of airflow when needed. This system prevents unstarts by increasing bypass airflow to compensate for reductions in the diffuser-exit airflow demand. References 1 to 4 indicate that large increases in the stability-bypass airflow may be provided without prohibitive amounts of airflow removal during normal operation; that is, the exit area is controlled to maintain a relatively constant pressure in the stability-bypass plenum. This exit-area variation might either be provided by an active control using shock position sensors or by a passive control using pressure-activated valves at the stability-bypass exit. These pressure-activated valves open in response to the pressure rise in the stability-bypass plenum caused by the forward moving terminal shock. To be most effective, the valves should be designed to maintain a nearly constant stability-bypass plenum pressure. Using a Mach 2.5 mixed-compression inlet with 40-percent internal contraction, reference 2 reported that several types of stability-bypass entrance configurations were capable of producing a

large stable airflow range if a constant-pressure stability-bypass exit control could be used. When these entrance configurations were used with pressure-activated valves (see refs. 3 and 4), the diffuser-exit airflow could be reduced as much as 28 percent from the optimum performance point without causing inlet unstart.

Experimental tests were conducted in the Lewis 10- by 10-Foot Supersonic Wind Tunnel to continue the evaluation of stability-bypass systems. The same types of stability-bypass systems as used in references 2 to 4 were investigated using an axisymmetric, Mach 2.5, mixed-compression inlet having 60 percent of the design supersonic area contraction occurring internally. Stability-bypass airflow was removed from the cowl side of the inlet throat region through several different entrance configurations. These entrance configurations used either a distributed porous surface, distributed educated slots, or a forward-slanted slot. The purpose of this report is to present the performance of two different size forward-slanted slot entrance configurations and to determine its suitability for use with pressure-activated valves designed to have a nearly constant pressure characteristic. The performance of the distributed educated and distributed porous configurations are reported in references 5 and 6, respectively. For the data reported herein remotely variable choked-exit plug assemblies were used to vary the stability-bypass flow.

Data were obtained at a free-stream Mach number of 2.50 and at a Reynolds number, based on the inlet cowl lip diameter, of 3.88×10^6. Some data were obtained at the maximum angle of attack before unstart.

U.S. customary units were used in the design of the test model and for recording and computing experimental data. These units were converted to the International System of Units for presentation in this report.

SYMBOLS

A	flow area, m^2
A_c	cowl lip capture area, 0.1758 m^2
AI	airflow index, $AI = 100 \left\{1 - \left[(W\sqrt{\theta}/\delta)_{min\ s} / (W\sqrt{\theta}/\delta)_{op}\right]_5\right\}$, percent
D_5	steady-state distortion, $\left[(P_{max} - P_{min})/P_{av}\right]_5$
d	distance from local surface, cm
H	annulus or rake height, cm
L	axial distance from upstream shoulder of slot entrance, cm
M	Mach number

m/m_0	mass-flow ratio
P	total pressure, N/m^2
p	static pressure, N/m^2
R_c	inlet cowl lip radius, 23.66 cm
r	radius, cm
SI_{cp}	constant pressure stability index, $SI_{cp} = 100 \left\{1 - \left[(W\sqrt{\theta}/\delta)_{\text{min s, cp}} / (W\sqrt{\theta}/\delta)_{\text{op}}\right]\right\}_5$, percent
T	total temperature, K
W	airflow, kg/sec
$W\sqrt{\theta}/\delta$	corrected airflow, kg/sec
x	axial distance from cone tip, cm
α	angle of attack, deg
δ	$P/(10.13\times10^4\ N/m^2)$
θ	T/288.2 K
θ_l	cowl lip position parameter, $\tan^{-1}\left[1/(x/R_c)\right]_{\text{cowl lip}}$
φ	circumferential position, deg

Subscripts:

av	average
bl	bleed
by	overboard bypass
cp	constant pressure
fc	forward cowl
l	local
max	maximum
min	minimum
min s	minimum stable inlet operating point
op	operation
sb	stability bypass
x	value at distance x

0 free stream

5 diffuser-exit station

APPARATUS AND PROCEDURE

Inlet Model

The inlet used in this investigation was a Mach 2.5, axisymmetric, mixed-compression type with 60 percent of the design supersonic area contraction occurring internally. The inlet capture area of 0.1758 square meter sized the inlet to match the airflow requirements of the J85-GE-13 engine at Mach 2.5 and at a free-stream total temperature of 390 K. The inlet was attached to a 0.635-meter-diameter cylindrical nacelle, in which either the engine or a coldpipe choked-exit plug assembly could be installed in the test section of the supersonic wind tunnel. For this study only the coldpipe was used. Figure 1 shows the test model installed in the wind tunnel test section.

Some of the basic inlet design details are presented in figure 2. Cowl and centerbody static-pressure distributions, inlet contours, and diffuser area variations are shown for the inlet design Mach number and centerbody position. External compression was accomplished with a 12.5° half-angle cone (fig. 3). Translation of this conical centerbody provided a varying contraction ratio to effect inlet restart. At design conditions, the cone tip oblique shock passed just ahead of the cowl lip spilling 0.25 percent of the capture mass flow. Internal compression was accomplished with the oblique shock generated by the 0° cowl lip and the two reflected oblique shocks plus local isentropic compression between the reflected shocks. As was pointed out in reference 8, the actual oblique shock reflection points were forward of the theoretically predicted points. The geometric throat of the inlet was located at $x/R_c = 3.475$ inlet radii (centerbody surface) where the theoretical average supersonic Mach number was 1.239 with a total-pressure recovery of 0.988. Behind the terminal shock the theoretical recovery was 0.975 at a Mach number of 0.8125.

The subsonic diffuser consisted of an initial throat region 4 hydraulic radii long with a 1° equivalent conical expansion followed by the main diffuser having an equivalent conical expansion of 8°. Two remotely controlled bypass systems were installed in the aft portion of the diffuser: (1) a high-response, sliding-louver overboard system for shock position control and (2) a low-speed ejector bypass for engine and nozzle cooling airflow. For the data reported herein both of these bypass systems were closed. The overboard bypass system leaked about 1 percent of the capture mass flow when nominally closed. The cascades placed at the entrance of the overboard bypass cavity (fig. 3) were found in reference 9 to minimize a resonance condition in the cavity. Vortex

generators were installed on the centerbody at inlet station 98.17 (fig. 3). Details of the vortex generator design are shown in figure 4.

The overall diffuser length from cone tip to compressor face was 7.72 cowl lip radii. Internal surface coordinates of the inlet in terms of the cowl lip radius are presented in table I. A more complete discussion of the inlet design characteristics is presented in reference 8.

Bleed regions were located in the throat region of the inlet on the cowl and centerbody surfaces. As shown in figure 5 the forward cowl bleed airflow was dumped directly overboard. The stability-bypass airflow (used to give the inlet a large stable airflow operating range) was removed through the entrance located on the cowl side of the throat region. Figures 3 and 5 illustrate the ducting of the stability-bypass flow through the cowling to the bypass pipes. The cowl stability-bypass and the centerbody bleed flows each used two coldpipe choked-plug assemblies. The remotely actuated plugs that were used to vary these bleed and bypass flows as well as the main duct flow are shown in figure 1(b).

The photographs and sketches of the test model show a bulky external profile. The bulky cowl was necessary to facilitate the major changes made to the stability bypass and associated ducting to vary the entrance configurations; hence it is not representative of flight type hardware.

Stability-Bypass Entrance and Bleed Region

The centerbody bleed region was composed of rows of normal holes (fig. 6). There were five rows of holes aft of the inlet throat and eight rows forward of the throat. The holes in the forward rows were arranged in a concentrated, staggered pattern. The intent of the staggering was to prevent bleed induced circumferential variations in the boundary layer.

A region of porous bleed on the forward cowl surface was provided for controlling the cowl side boundary-layer development. This bleed region as shown in figure 7 comprised a concentrated hole pattern identical to that used for the centerbody bleed region. The holes were 0.3175 centimeter in diameter and were drilled normal to the local inlet surface. The nominal porosity of 40-percent was achieved by locating the holes on 0.4673-centimeter centers. Nominal thickness of the metal in the bleed regions was equal to the hole diameter.

A single centerbody bleed pattern was used for both configurations tested as shown in figure 8. This pattern, formed by filling the selected rows of bleed holes and identical to the final pattern presented in reference 6, provided optimum inlet performance when used with a porous stability-bypass entrance configuration.

The bleed characteristics contained in references 10 to 12 were used to design not only the cowl and centerbody bleed regions but also the forward slanted slot stability-bypass entrance configurations that were tested. The two slot designs tested are shown in figure 7; the small slot was constructed from the large slot by adding an insert piece shown by the crosshatched section of the figure. The large slot entrance was designed to be capable of removing about 23 percent of the inlet capture mass-flow ratio; the small slot was designed to have about one-half the airflow removal capability. Each slot entrance was flush with the local inlet surface contour, and the slot passage proceeded downstream at a 20° angle. The upstream corner of each slot was sharp, and the downstream lip before rounding was located at the inlet geometric throat. A rounded lip was selected for testing on the basis of the effects of lip shape reported in reference 2.

The two complete forward-slanted slot configurations tested are shown in figure 8. The selected forward cowl and centerbody bleed patterns were constructed by filling in the appropriate rows of normal holes.

Instrumentation

Static-pressure distributions along the top centerline of the inlet cowl and centerbody were measured by the axially located static-pressure instrumentation presented in tables II and III. The main-duct total-pressure instrumentation (fig. 9) was used to determine the local flow profiles through the inlet and subsonic diffuser. The axial locations of these total-pressure rakes are shown in figure 3. Overall inlet total-pressure recovery and distortion were determined from the six 10-tube total-pressure rakes that were located at the diffuser exit (fig. 9(b)). Each rake consisted of six equal-area-weighted tubes with additional tubes added at each side of the extreme tubes in radial positions corresponding to an 18-tube area-weighted rake.

The main duct airflow, the stability-bypass airflow, and the centerbody bleed airflow were determined from static-pressure measurements and the appropriate coldpipe choked-plug areas. Bleed flow through the forward cowl bleed region was determined from the measured total and static pressures (fig. 9(c)) and the bleed exit area.

Stability-bypass total pressure was obtained from two total-pressure rakes that were located in the bypass plenum at an x/R_c of 4.086 inlet radii. Pressures from these rakes were averaged to obtain the stability-bypass recovery. Centerbody bleed and overboard-bypass total pressures were each measured by a single probe as indicated in figure 9(c).

Forward-slanted slot instrumentation is presented in figure 10. Total-pressure rakes were located just forward and aft of the upstream corner of each slot and in the slot passage. The rakes were circumferentially displaced to avoid flow interference.

Static pressures were also measured axially along each slot, and the axial locations are shown in figure 10.

PERFORMANCE ANALYSIS TECHNIQUE

This section of the report introduces stylized plots (fig. 11) that are typical of actual inlet stability data presented later. These plots are used to explain the data presentation and to show the method used to construct a final performance plot. Various performance conditions have been labeled in figure 11 to aid in the discussion.

The stability-bypass performance is shown in figure 11(a) where the total-pressure recovery is presented as a function of the mass-flow ratio of the stability bypass. The series of straight solid lines (A'AB, C'CD, etc.) represent the bypass performance obtainable with several different fixed bypass exit areas. Corresponding inlet performance is presented in figure 11(b) by a series of standard diffuser-exit total-pressure recovery against mass-flow ratio curves. The diffuser-exit mass-flow ratio, of course, reflects the changes in bypass mass-flow ratio and also changes in forward cowl and centerbody bleed mass-flow ratios. Each solid line curve represents the performance obtainable with a fixed bypass exit area and corresponds to the solid straight line of identical labeling in figure 11(a). Each of these curves is generated by reducing the inlet diffuser-exit corrected airflow from a supercritical value and thus causing the inlet terminal shock to move upstream until unstart occurs. By this mode of operation, loci (dashed curves) of supercritical stability-bypass airflow (A'A C'C E'E G'G) and minimum stable bypass airflow (BDFH) are obtainable. For a given bypass exit area all the supercritical inlet operating points have approximately the same bypass mass-flow and pressure-recovery values. Only when the terminal shock is in the vicinity of the stability-bypass entrance region will shock pressurization occur, causing increases in the bypass mass flow and pressure recovery toward their respective minimum stable limit values. Thus, for example, all the inlet operating points between A' and A of figure 11(b) will have the same stability-bypass performance point which is labeled as A'A in figure 11(a).

To assess inlet stability, it is necessary to look at the change in the diffuser-exit corrected airflow, which is a function of both diffuser-exit mass-flow ratio and total-pressure recovery. Figure 11(c) presents inlet stability, expressed as an airflow index, for the same conditions of figures 11(a) and (b). Values of airflow index (AI) represent the percentage change in corrected airflow between any inlet operating condition and the minimum recorded corrected airflow at point H. Figure 11(c) thus illustrates the amount of stable margin available if the stability-bypass exit area can be varied to guide the inlet operation from any operating condition to an unstart at point H. If a fixed

exit area were used to obtain the large stability-bypass airflow available at point H (fig. 11(a)), a prohibitively large amount of bypass airflow would be removed from the diffuser flow at supercritical conditions (point G). If the fixed exit area were reduced to obtain an acceptably low level of supercritical bypass airflow (point C), the amount of bypass airflow and consequently the stable margin at the minimum stable condition (point D) would also be reduced. Similar bypass characteristics are reported in references 1 to 4.

Data such as that presented in figure 11(a) to (c) show the characteristic performance of an inlet with a stability-bypass entrance. Since a performance assessment from these plots is difficult, a single operating line was chosen to represent the configuration performance. One end of the line represents a high-performance operating point that matches the inlet and an assumed engine and will be called the match point (point A for example). The match point was chosen to have a high inlet recovery and a small amount of cowl side airflow removal for boundary-layer control. The other end of the operating line (the minimum stable point) was chosen by the selection of an ideal variable exit area, one that would provide a constant pressure in the bypass plenum as the inlet operated from the match point to the minimum stable point. This variable exit area provides the maximum attainable stability (points A to M in fig. 11(a)). Reference 4 reports a pressure-activated valve that varied the stability-bypass exit area to maintain an almost constant bypass plenum pressure. Thus, the selection of a constant pressure characteristic for a stability-bypass exit control is a valid technique for assessing inlet stability performance.

The inlet stability margin that is produced by a constant-pressure bypass-exit-area control is expressed as a stability index SI_{cp}. Figure 11(d) presents the constant pressure stability index for all of the operating points of figures 11(a) to (c). Note that the selected match point stability (A to M in figs. 11(a) to (c)) is now represented by a single point A. The values of stability index at any operating point represent the percentage change in corrected airflow between that point and a minimum stable point that is reached only along a line of constant stability-bypass pressure recovery (A to M in fig. 11(a)). When the inlet operating point has a stability-bypass recovery lower than that of the absolute minimum stable point (H in fig. 11(a)), the absolute minimum stable point is used to compute the stability index. Therefore, the stability index for the lower bypass recovery conditions in figure 11(d) becomes identical to the airflow index in figure 11(c). Although the stability index is defined in terms of corrected airflow, that is,

$$SI_{cp} = 100\left[1 - \frac{\left(\frac{W\sqrt{\theta}}{\delta}\right)_{\text{min s, cp}}}{\left(\frac{W\sqrt{\theta}}{\delta}\right)_{op}}\right] \tag{1}$$

it was easier in practice to determine values of stability index directly from curves of airflow index by means of the following equation:

$$SI_{cp} = 100\left(\frac{AI_{op} - AI_{min\ s,\,cp}}{100 - AI_{min\ s,\,cp}}\right) \tag{2}$$

where AI_{op} is the airflow index at any inlet operating condition and $AI_{min\ s,\,cp}$ is the airflow index at the corresponding minimum stable point assuming a constant bypass recovery is maintained.

Constant-pressure stability index levels may be converted into typical inlet performance plots like that of figure 11(g) by means of figures 11(e) and (f). Figure 11(e) presents the constant pressure stability index that was computed for each inlet operating condition as a function of inlet total-pressure recovery. A selected inlet total-pressure recovery may be represented in figure 11(e) as a vertical line (IJKL). (Note that point A is no longer necessarily the selected match point. The choice of inlet recovery and the amount of performance bleed will dictate the match point.) The intersection of this line with the lines of constant bypass exit area indicate the constant-pressure stability indices available at the selected inlet recovery for the various bypass exit areas. A replot of these data in figure 11(f) shows the amount of stability margin that is available when operating the inlet at the selected match recovery as a function of the various amounts of initial total forward cowl bleed and stability-bypass mass flow. Any of the data points in figure 11(f) may be converted into a typical inlet performance plot. Point J, for example, is shown in figure 11(g) and is determined by the previously selected inlet recovery and the initial amount of total mass flow removed through the cowl surface. If point J represents critical inlet performance, then supercritical performance is represented by a vertical line extended below point J. The constant-pressure stability index for point J as determined by equation (1) is represented by the airflow difference between two corrected airflow lines; one through the selected match point $(W\sqrt{\theta}/\delta)_{op}$ and the other $(W\sqrt{\theta}/\delta)_{min\ s,\,cp}$ intersecting the locus of minimum stable condition as on the inlet performance map (fig. 11(b)). For convenience inlet performance between the match point and the minimum stable point is represented by a straight line. Intermediate points could be determined by using figures 11(a) to (d).

RESULTS AND DISCUSSION

The results of this investigation are presented in two parts: the stability performance of the two configurations and the unstart angle-of-attack tolerance of the configurations.

Stability Performance

The overall characteristic performance curves for the large forward-slanted slot configuration are presented in figure 12. Cowl and centerbody surface static-pressure distributions and total-pressure profiles at the various survey stations are presented in figure 13 for minimum stable operating conditions and in figure 14 for representative supercritical operating conditions. Only profiles for rake 5 of the six diffuser-exit rakes will be presented herein because this profile was representative of those of the other rakes. Note that wherever possible throughout this report consistency has been maintained in the figure symbols; that is, the same symbol used to represent a particular fixed bypass exit area in the stability-bypass-performance curves (e.g., fig. 12(a)) has also been used in the accompanying inlet performance curves (e.g., figs. 12(b) to (i)) and in the pressure distribution and profile figures (e.g., figs. 13 to 14).

The stability bypass performance curves of figure 12(a) reveal that an unexpected aerodynamic phenomenon concerning the large slot occurred at the higher values of bypass mass-flow ratio. As discussed in the PERFORMANCE ANALYSIS TECHNIQUE section, as the inlet terminal shock is moved upstream in the throat region toward its minimum stable position, the stability bypass mass-flow ratio and pressure recovery nominally increase toward their respective limiting values. Figure 12(a) indicates that at the higher bypass mass-flow ratios, this trend reversed itself; that is, the mass flow and recovery levels took on their maximum values at the supercritical conditions, and both then decreased as minimum stable was approached. This reversal phenomenon would appear to limit the useful stability bypass mass-flow ratio range for the large slot configuration to about 0.14 or less, as it would be difficult to design an exit area control that could follow the bypass performance characteristics of figure 12(a). The curves of figure 12(a) indicate that high-pressure recovery levels were realized with the large slot configuration, which makes such an entrance configuration attractive when potential bleed drag penalties are considered.

The bypass reversal trend discussed can also be seen in the inlet performance curves of figure 12(b). At the operating points corresponding to the higher stability-bypass mass flows, the diffuser-exit mass-flow ratio increased as minimum stable was approached. The figure also indicates that inlet operation with no stability bypass flow (corresponding to the square symbol) resulted in a minimum stable pressure recovery of less than 0.90. This decreased inlet recovery performance resulted in a stability performance penalty for the large slot configuration (fig. 12(f)). The stability index curve indicates that to achieve a large amount of inlet stability it is necessary to increase the total forward cowl bleed and stability bypass mass-flow ratio at the initial operating point to 0.045. Such increased amounts of flow removal through the cowl surface result in a bleed drag penalty being paid to provide large amounts of inlet stability.

It must be noted that, to construct figure 12(f), an initial inlet pressure recovery level had to be chosen. Comparing the results of all tests of this inlet with various stability-bypass entrance configurations (refs. 5 and 6) showed that the 0.89 pressure recovery was at a representative level. The inability of the large slot configuration to provide this recovery level without any stability bypass flow as previously pointed out resulted in the poor stability performance shown in figure 12(f) for the lower amounts of mass flow removal through the cowl.

The throat exit rake profiles for both minimum stable (fig. 13(d)) and representative supercritical operating conditions (fig. 14(d)) indicate that at the higher stability bypass flows the diffuser flow tended to separate from the centerbody surface in the throat region. This incipient separation appeared to occur regardless of terminal shock position. Apparently the centerbody bleed pattern was not sufficient to maintain attached flow at the higher flow removal rates. The retarded flow was evident at the diffuser-exit station (figs. 13(f) and 14(f)) and was probably the cause of the corresponding reduced inlet pressure recovery levels experienced (see fig. 12(b)). As reference 6 points out, the centerbody bleed pattern used can have a large effect on the stability-bypass performance achieved. Perhaps a further tailoring of the centerbody bleed could have eliminated the centerbody flow separation problem and thus increased the stability performance achieved. However, no such bleed refinement was undertaken as the purpose of this study was only to show the feasibility of using a constant-pressure stability-bypass system to increase the inlet's stable operating range.

The mechanism responsible for the unexpected trend reversal of the stability-bypass mass-flow ratio and recovery can be understood from a study of the slot rake profiles and static-pressure distributions along the upstream slot surface. The profiles of slot rake B corresponding to minimum stable inlet conditions (fig. 13(h)) clearly show that the bypass flow could not negotiate the 20° turn into the slot entrance and that it separated from the cowl surface regardless of the amount of bypass flow. The rake B profiles for the representative supercritical operating points (fig. 14(h)) also indicate that the flow always separated except for the point corresponding to the largest bypass exit area where a fully developed attached profile is shown. Apparently, the separation of the bypass flow as it entered the slot passage was adversely affecting the attainable stability-bypass performance by reducing the effective slot opening area. The profiles for rake C (figs. 13(i) and 14(i)) indicate the flow had not always reattached before reaching that station. If the minimum stable rake B profiles are compared (fig. 13(h)) it can be seen that the separated zone height appeared to remain about the same regardless of the amount of bypass flow. However, the height of the separated zone appeared to continually decrease with increased bypass flow at supercritical conditions (fig. 14(h)). Thus, at the higher bypass flows, the size of the separated region appeared to grow as the terminal shock moved upstream from a supercritical position into the throat region

for a given bypass exit area. The growth of the separated zone further restricted the amount of bypass flow that could enter the slot. The static-pressure distributions on the upstream surface of the slot passage (figs. 13(j) and 14(j)) indicate that the separation zone so constricted the passage area that the bypass flow actually accelerated to supersonic conditions and then shocked out to subsonic conditions in the passage.

The development of the separated zone with changing terminal shock position and its effect on slot performance can be easily seen in figure 15. This figure presents the pressure distributions and rake profiles corresponding to operation at the largest bypass exit area and represents the movement of the terminal shock from a supercritical downstream position to its minimum stable limit position. The slot rake B profiles (fig. 15(h)) indicate that, for the most supercritical terminal shock positions, the bypass flow remained attached as it entered the passage as shown in sketch (a):

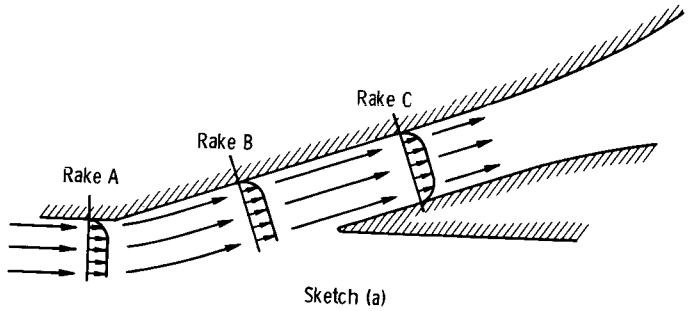

Sketch (a)

However, further movement of the terminal shock resulted in the flow separation and resultant lessening in effective slot entrance area. The reduced amount of bypass flow entering the slot passage then accelerated to supersonic conditions and finally shocked out to subsonic exit conditions as shown in sketch (b):

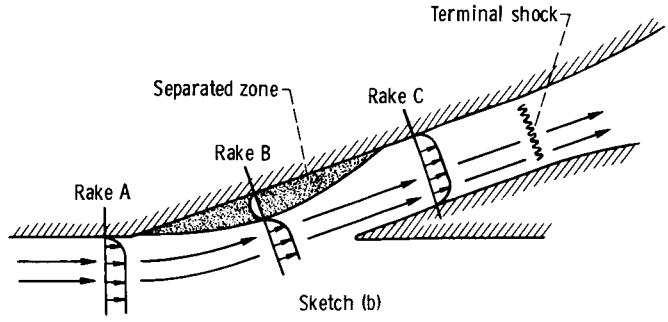

Sketch (b)

The corresponding slot passage static-pressure distributions (fig. 15(j)) reveal that, as the terminal shock moved further upstream, the strength of the shock in the slot passage became stronger and thus resulted in the decrease in bypass recovery as minimum stable was approached.

The separation problem encountered with the large slot configuration severely limited the attainable stability performance. If the separation at the slot entrance could have been eliminated, the large slot configuration could possibly have been a superior stability bypass system. As figure 12(a) indicates, even with the flow separation present, the slot could pass a maximum of about 0.22 bypass mass-flow ratio and, further, the pressure recovery levels achieved before the trend reversal occurred were high. Perhaps the separation problem might have been eliminated if a curved upstream slot leading edge rather than the sharp leading edge had been used.

The overall performance curves for the small slot configuration are presented in figure 16. The stability-bypass performance curves (fig. 16(a)) reveal that a similar trend reversal occurred for the highest bypass exit area. However, it can also be seen that the trend righted itself and both bypass mass flow and pressure recovery increased in value to their respective minimum stable limits. The static-pressure distributions and rake profiles for various selected operating points presented and discussed later will show that a similar separation at the upstream edge of the slot entrance as experienced by the large slot configuration was responsible for the observed trend reversal.

The bypass performance curves (fig. 16(a)) also reveal that pressure recovery levels in excess of 0.70 were achieved for minimum stable conditions. The 0.70 recovery level represents a slight increase over the maximum level recorded for the large slot configuration (0.66). Both levels do exceed the maximum performance obtained for a series of distributed porous stability-bypass entrance configurations tested (ref. 6), the maximum recorded recovery there being 0.64.

The corresponding inlet performance curves (fig. 16(b)) indicate that the small slot configuration, unlike the large slot configuration, could achieve diffuser-exit recoveries in excess of 0.90 without any flow removal through the bypass system. The effect of this increased inlet performance is evident in figure 16(f) where it can be seen that large amounts of inlet stability are available for small amounts of total forward cowl and stability-bypass mass-flow removal. A total amount of mass-flow ratio removal of about 0.02 would result in a constant-pressure stability index of 18.5 percent. This can be compared with the large slot stability performance already discussed where it was ascertained that, in order to achieve a stability index of 17.0 percent, approximately 0.045 mass-flow ratio had to be removed through the cowl surface (fig. 12(f)). The levels of stability index achieved by this configuration can be largely attributed to the diffuser-exit pressure-recovery performance (fig. 16(b)). As the bypass area was increased, the recovery at minimum stable conditions continually increased reaching a

maximum value of 0.944.

The static-pressure distributions and rake profiles are presented in figure 17 for minimum stable conditions and in figure 18 for representative supercritical operating conditions. In addition, similar distributions and profiles are presented in figure 19 for operation at the largest bypass exit area. As noted previously, the slot rake profiles and upstream slot static-pressure distributions indicate that a flow separation in the vicinity of the bypass entrance was again responsible for the trend reversal. The rake D profiles of figure 19(h) clearly show that as the inlet terminal shock moved upstream into the throat region, the flow separated from the upstream slot surface. The corresponding slot rake E profiles (fig. 19(i)) reveal the flow had always reattached before reaching that station. The slot surface static-pressure distributions of figure 19(j) indicate that the bypass flow accelerated to supersonic conditions and then shocked out to subsonic conditions before reaching the bypass exit.

It is difficult to determine from the available data what caused the resumption of the normal bypass performance as the terminal shock moved forward in the throat after the initial trend reversal. From the limited data available at rake D (fig. 19(h)), it appears that once the separation region was established it did not grow appreciably in height. Thus, as the terminal shock moved forward in the throat region, it possibly caused larger slot pressures which in turn resulted in more mass flow through the slot, which retained the same effective entrance area. Examination of the profiles of slot rake D for minimum stable conditions (fig. 17(h)) and representative supercritical conditions (fig. 18(h)) reveals that with the exception of operation at the largest bypass exit area, a separation of roughly the same height was present regardless of inlet conditions. The effect of the separation on the small slot thus appears to have been to reduce the effective entrance area of the slot. However, at the most supercritical operating condition corresponding to the largest exit area, the ability of the bypass flow to remain attached resulted in increased flow through the bypass system. A forward movement of the terminal shock reestablished the separation zone and thus caused the reduction in bypass flow. The slot flow separation observed in all probability lessened the stability performance exhibited by the small slot configuration although not to the extent it hindered the performance of the large slot. If the separation could have been eliminated, an increased range of stability bypass mass-flow ratio may have been realized.

A small scale centerbody boundary-layer separation was noted for the small slot configuration at the minimum stable conditions corresponding to the largest stability-bypass mass flow. The boundary-layer rake profiles of figure 17(c) show the development of the separated region as the bypass flow was increased. From the corresponding cowl and centerbody surface static-pressure distributions (figs. 17(a) and (b)), it can be seen that the terminal shock could be positioned well upstream of the geometric throat before unstart. The centerbody separation appeared to be of a shock induced nature and was similar to a separation phenomenon reported in references 5 and 6 for the same

general supersonic inlet model but with varying stability bypass entrance configurations. Reference 8 also noted the separation and indicated that it was shock induced because the terminal shock could be positioned in the vicinity of the forward-most bleed location. Certainly, the static-pressure profiles (figs. 17(a) and (b)) do indicate that the shock was positioned close to the upstream limit of the bleed location. The corresponding throat exit rake profiles (fig. 17(d)) indicate only a slight effect of the separation in the form of reduced recovery levels near the centerbody surface. However, no effect can be noticed at the diffuser exit station (fig. 17(f)), and apparently the separation was confined to the throat region.

To make a direct comparison of the stability performance of the two configurations using the constant pressure stability index concept, figures 12(f) and 16(f) must be consulted. As noted previously, figure 12(f) indicates that optimum stability performance of the large slot configuration occurred when about 0.045 total forward cowl bleed and stability-bypass mass-flow ratio was removed through the cowl surface at the initial operating point. The stability index of 17.0 percent would result in a minimum stable operating point of 0.93 diffuser-exit pressure recovery and 0.80 mass-flow ratio. From figure 12(a) the corresponding bypass plenum recovery level maintained would be about 0.45, and the increase in bypass mass-flow ratio before unstart would be about 0.11. The optimum small slot stability index performance of 18.5 percent occurred when the total mass-flow ratio removal through the cowl surface was only about 0.02 (fig. 16(f)). The corresponding minimum stable point would be 0.94 pressure recovery and 0.82 mass-flow ratio. According to figure 16(a) a bypass plenum recovery of about 0.50 would be maintained with an allowable increase in stability bypass mass-flow ratio of about 0.10. The approximate operating curves for the two configurations shown in figure 20 indicate that the small slot configuration offered the more attractive stability performance characteristics. From the initial operating point, the small slot configuration could bypass only 0.01 less mass-flow ratio before unstart than could the large slot configuration, and it could achieve a higher diffuser exit recovery before unstart. Also the small slot configuration required approximately 0.025 less bleed and bypass mass-flow ratio to achieve the desired recovery of 0.89 at the operating point. In addition, the bypass plenum recovery level maintained was about 0.05 higher for the small slot configuration. The combination of less initial flow removal and higher bypass recovery levels would result in a smaller bleed drag penalty for the small slot configuration.

Unstart Angle-of-Attack Tolerance

The unstart angles of attack for various initial inlet operating conditions for the two configurations are indicated on the appropriate inlet performance curves (figs. 12(b) and 16(b)). The angles listed represent the maximum steady-state angle of attack the par-

ticular inlet configuration could tolerate before the occurrence of unstart. All angles of attack given herein correspond to conditions of no flow through the stability bypass entrance. The only cowl side flow removal was through the forward cowl bleed region, and thus all bleed flows were for performance.

In a separate study of the same inlet but with performance bleed only (ref. 13), it was determined that unstarts at angle of attack were caused by an overcompression of the flow field on the leeward side of the inlet. This overcompression resulted in a local choking of the flow upstream of the geometric throat and subsequent unstart. Figure 21 presents the static-pressure distributions for both the cowl and centerbody surfaces for the small forward-slanted slot configuration at 3.35° operation for initial supercritical inlet conditions. For reference the initial 0 angle-of-attack operating point pressure distributions are also shown. The distributions presented are typical of all those recorded for angle-of-attack operation. The cowl surface distribution of figure 21(a) reveals a region forward of the geometric throat where the pressure ratio rose well above the sonic value of 0.5283 (assuming isentropic conditions). In addition, the profiles indicate the terminal shock was well downstream of the geometric throat. Thus, it appears as though a leeward side overcompression and resulting local flow choking caused the angle-of-attack unstarts.

The unstart angles of attack achieved by the two configurations varied from 2.99° to 3.35°, depending on the initial inlet operating conditions. These angles are commensurate with those reported in references 8 and 13 for the same inlet with varying performance bleed configurations. Thus, it appears as though the inclusion of a stability-bypass system with the required entrance region did not affect the inlet's basic angle-of-attack tolerance. This was the expected result because the overcompression and local choking occurred upstream of the stability-bypass entrance.

SUMMARY OF RESULTS

An experimental program was conducted in the Lewis 10- by 10-Foot Supersonic Wind Tunnel to evaluate the effectiveness of two forward-slanted slot throat stability-bypass entrance configurations in providing an increased inlet stable airflow operating range. The inlet used in this study was an axisymmetric, mixed compression type with 60 percent of the supersonic area contraction occurring internally at the design Mach number of 2.50.

The following results were obtained:

1. A large stable airflow operating range could be provided for the inlet operating at a high performance condition by maintaining a nearly constant plenum pressure in an inlet stability-bypass system. From initial inlet operating conditions of 89 percent, diffuser-exit pressure recovery, and a total forward cowl bleed and stability-bypass

mass-flow ratio of 0.02, the diffuser-exit corrected airflow could be reduced 18.5 percent before unstart for the small forward slanted slot configuration. The large forward-slanted slot configuration provided a 17.0-percent reduction in corrected airflow if the initial total forward cowl bleed and stability-bypass mass-flow ratio was increased to 0.045.

2. At the higher stability-bypass flows, both of the slot configurations experienced a flow separation in the slot entrance. This separation restricted the useful stability operating range of the configurations to the lower stability bypass airflow range.

3. Inlet unstart angle-of-attack tolerance for the configurations varied from 2.99° to 3.35° depending on the initial inlet conditions. These levels were commensurate with the results determined for the same inlet without the inclusion of a throat stability-bypass system. In all cases the unstarts incurred from angle-of-attack operation resulted from local flow choking forward of the geometric throat on the leeward side of the inlet.

Lewis Research Center,
National Aeronautics and Space Administration,
Cleveland, Ohio, December 12, 1973,
501-24.

REFERENCES

1. Sanders, Bobby W.; and Cubbison, Robert W.: Effect of Bleed-System Back Pressure and Porous Area on the Performance of an Axisymmetric Mixed-Compression Inlet at Mach 2.50. NASA TM X-1710, 1968.

2. Sanders, Bobby W.; and Mitchell, Glenn A.: Throat-Bypass Bleed Systems for Increasing the Stable Airflow Range of a Mach 2.50 Axisymmetric Inlet with 40-Percent Internal Contraction. NASA TM X-2779, 1973.

3. Sanders, Bobby W.; and Mitchell, Glenn A.: Increasing the Stable Operating Range of a Mach 2.5 Inlet. Paper 70-686, AIAA, June 1970.

4. Mitchell, Glenn A.; and Sanders, Bobby W.: Pressure-Activated Stability-Bypass-Control Valves to Increase the Stable Airflow Range of a Mach 2.5 Inlet with 40-Percent Internal Contraction. NASA TM X-2972, 1974.

5. Shaw, Robert J.; Mitchell, Glenn A.; and Sanders, Bobby W.: Distributed Educated Throat Stability Bypass to Increase the Stable Airflow Range of a Mach 2.5 Inlet with 60-Percent Internal Contraction. NASA TM X-2975, 1974.

6. Shaw, Robert J.; Mitchell, Glenn A.; and Sanders, Bobby W.: Distributed Porous Throat Stability Bypass to Increase the Stable Airflow Range of a Mach 2.5 Inlet with 60-Percent Internal Contraction. NASA TM X-2974, 1974.

7. Mitchell, Glenn A.; Sanders, Bobby W.; and Shaw, Robert J.: Throat Stability-Bypass Systems to Increase the Stable Airflow Range of a Mach 2.5 Inlet with 60-Percent Internal Contraction. NASA TM X-2976, 1974.

8. Cubbison, Robert W.; Meleason, Edward T.; and Johnson, David F.: Effect of Porous Bleed in a High-Performance Axisymmetric, Mixed-Compression Inlet at Mach 2.50. NASA TM X-1692, 1968.

9. Coltrin, Robert E.; and Calogeras, James E.: Supersonic Wind Tunnel Investigation of Inlet-Engine Compatibility. Paper 69-487, AIAA, June 1969.

10. McLafferty, George: A Stepwise Method for Designing Perforated Supersonic Diffusers. Rep. R-12133-5, United Aircraft Corp., Nov. 17, 1949.

11. McLafferty, George: Study of Perforation Configurations for Supersonic Diffusers. Rep. R-53372-7, United Aircraft Corp., Dec. 1950.

12. McLafferty, George; and Ranard, E.: Pressure Losses and Flow Coefficients of Slanted Perforations Discharging from Within a Simulated Supersonic Inlet. Rep. R-0920-1, United Aircraft Corp., 1958.

13. Choby, David A.: Tolerance of Mach 2.50 Axisymmetric Mixed-Compression Inlets to Upstream Flow Variations. NASA TM X-2433, 1972.

TABLE I. - INLET INTERNAL SURFACE COORDINATES

(a) Centerbody

Axial distance from cone tip, x/R_c, inlet radii	Radial distance, r/R_c, inlet radii	Axial distance from cone tip, x/R_c, inlet radii	Radial distance, r/R_c, inlet radii
0	0	4.563	0.588
(a)	(a)	4.724	.566
2.885	.640	5.161	.498
2.924	.649	5.261	.481
2.952	.655	5.361	.462
3.017	.667	5.461	.444
3.081	.678	5.561	.418
3.124	.684	5.661	.409
3.178	.691	5.761	.396
3.221	.696	5.861	.373
3.237	.700	5.961	.357
3.306	.703	6.061	.341
3.349	.705	6.161	.327
3.403	.707	6.261	.313
3.435	.708	6.361	.299
3.446	↓	6.461	.285
3.457	↓	6.561	.272
3.468	↓	6.661	.260
3.478	.707	6.761	.250
3.489	.706	6.861	.243
3.543	.702	8.961	.240
3.596	.697	7.061	.239
3.650	.691	Cylinder	
3.865	.670	7.946	0.239
3.972	.660		
4.079	.649		
4.120	.644		
4.187	.636		
4.240	.635		
4.294	.623		
4.402	.609		

[a] 12.5^{o} Half angle conical section.

TABLE I. - Concluded. INLET INTERNAL SURFACE COORDINATES

(b) Cowl

Axial distance from cone tip, x/R_c, inlet radii	Radial distance, r/R_c, inlet radii	Axial distance from cone tip, x/R_c, inlet radii	Radial distance, r/R_c, inlet radii
2.009	1.000	4.267	0.906
2.156	↓	4.277	.905
2.297		4.384	.903
2.383		4.545	.902
2.469		4.706	.902
2.491		4.868	.903
2.512		5.029	.904
2.566	.999	5.093	.904
2.630	.997	5.161	.905
2.695	.995	5.261	.907
2.738	.994	5.361	.910
2.811	.992	5.461	.913
2.860	.989	5.561	.916
2.885	.988	5.661	.917
2.924	.986	5.761	.918
2.952	.985	Cylinder	
3.017	.981		
3.081	.979	6.235	0.918
3.124	.976	Bypass gap	
3.178	.972		
3.221	.971	6.845	0.887
3.237	.966	6.861	.887
3.306	.963	6.961	.885
3.350	.960	7.061	.882
3.403	.955	7.161	.879
3.435	.953	7.261	.873
3.446	.952	7.361	.868
3.457	.951	7.461	.864
3.468	.951	7.561	.863
3.478	.950	7.661	.862
3.489	.949		
3.543	.945	Cylinder	
3.596	.942		
3.650	.939	7.946	0.862
3.756	.932		
3.863	.925		
3.970	.919		
4.088	.913		
4.093	.913		
4.189	.909		

TABLE II. - INTERNAL COWL SURFACE STATIC-PRESSURE

TAP LOCATIONS ALONG TOP CENTERLINE

Axial distance from cone tip, x/R_c, inlet radii	
Large forward-slanted slot	Small forward-slanted slot
2.983	2.983
3.090	3.090
3.160	3.160
3.195	3.195
3.230	3.230
3.265	3.265
3.298	3.298
3.566	3.343
3.589	3.389
3.621	3.566
3.662	3.589
3.739	3.621
3.818	3.662
3.961	3.739
4.254	3.818
	3.961
	4.254

TABLE III. - CENTERBODY STATIC PRESSURE

TAP LOCATIONS ALONG TOP CENTERLINE

Axial distance from cone tip, x/R_c, inlet radii		
2.806	3.367	3.854
2.920	3.402	3.906
3.022	3.440	3.961
3.135	3.470	4.067
3.173	3.516	4.174
3.206	3.573	4.331
3.242	3.635	
3.272	3.691	
3.315	3.741	
3.332	3.798	

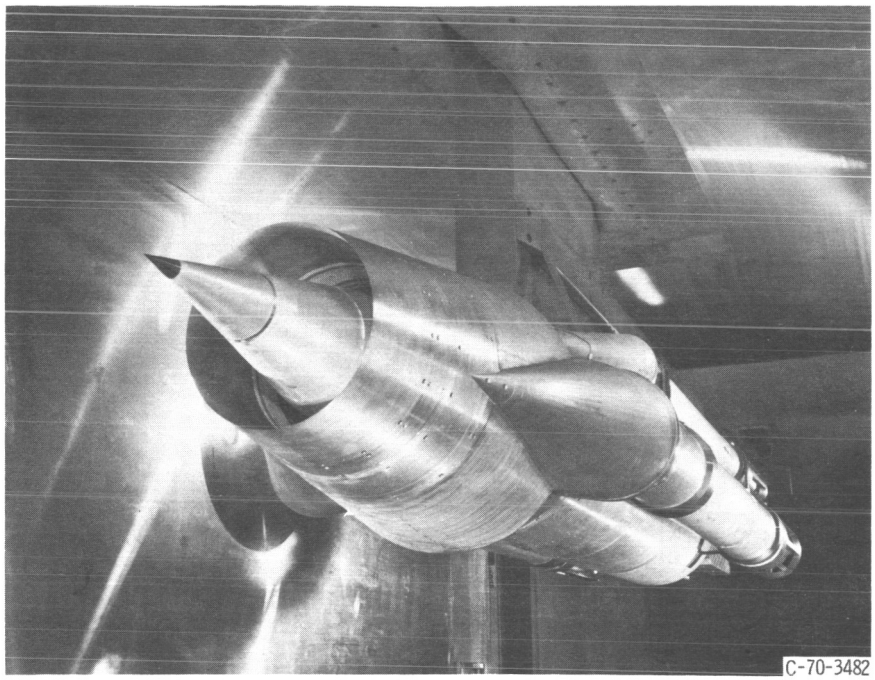

(a) Front view.

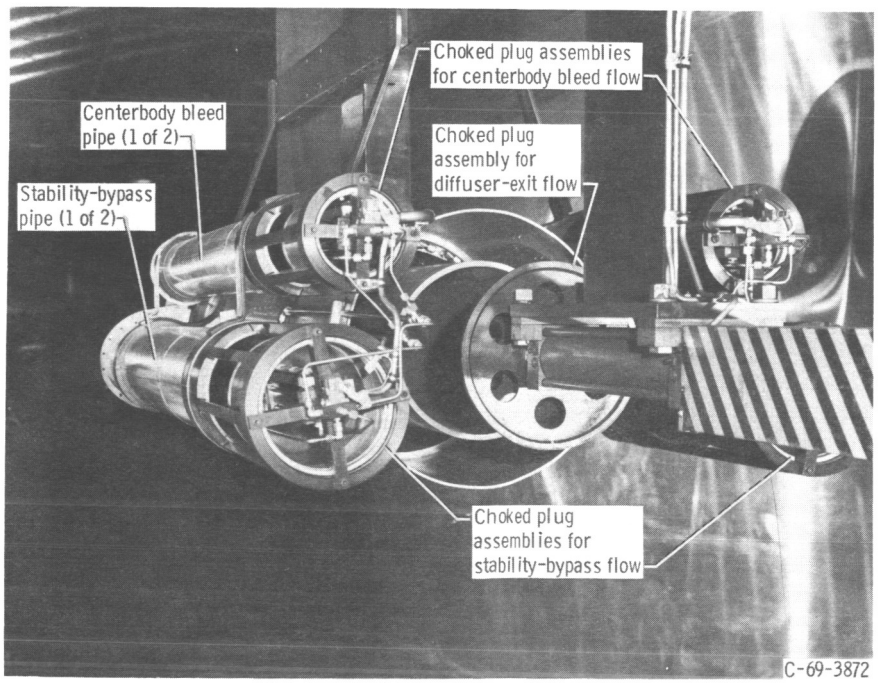

(b) Rear view.

Figure 1. - Model installed in wind tunnel.

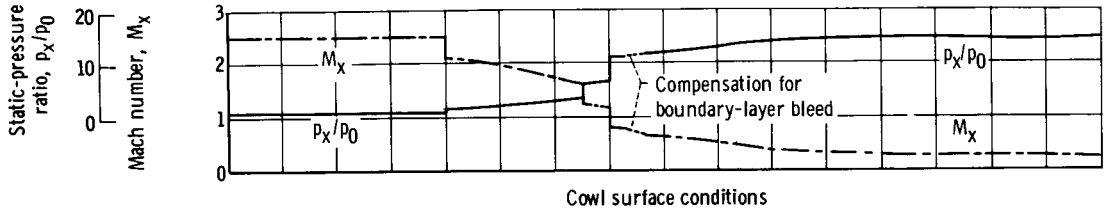

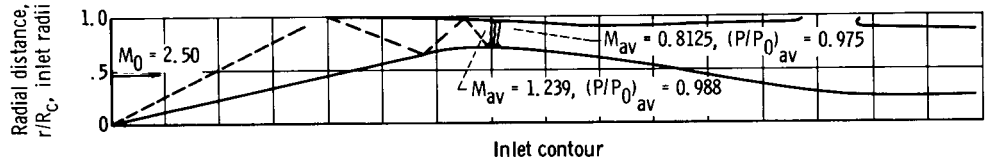

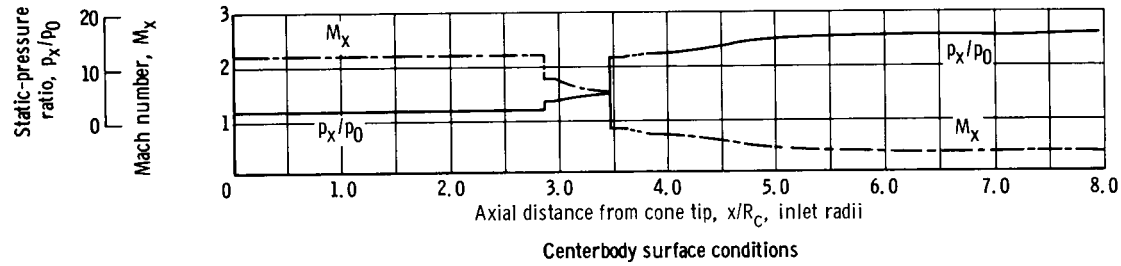

(a) Inlet dimensions and theoretical flow conditions.

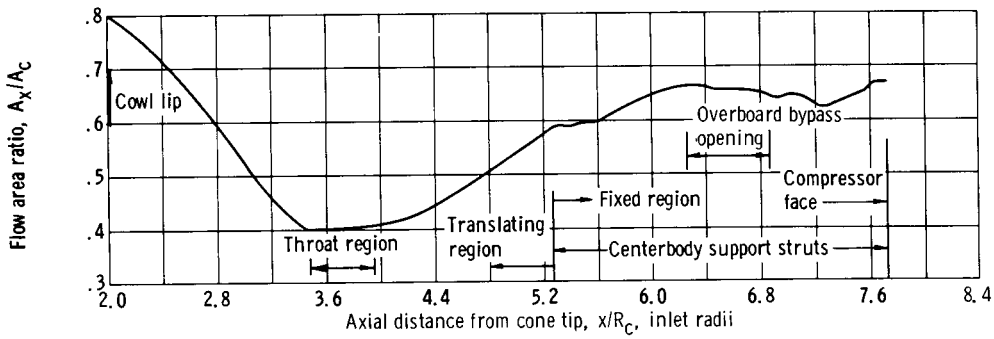

(b) Diffuser area variation for θ_l, 26.72°.

Figure 2. - Aerodynamic details.

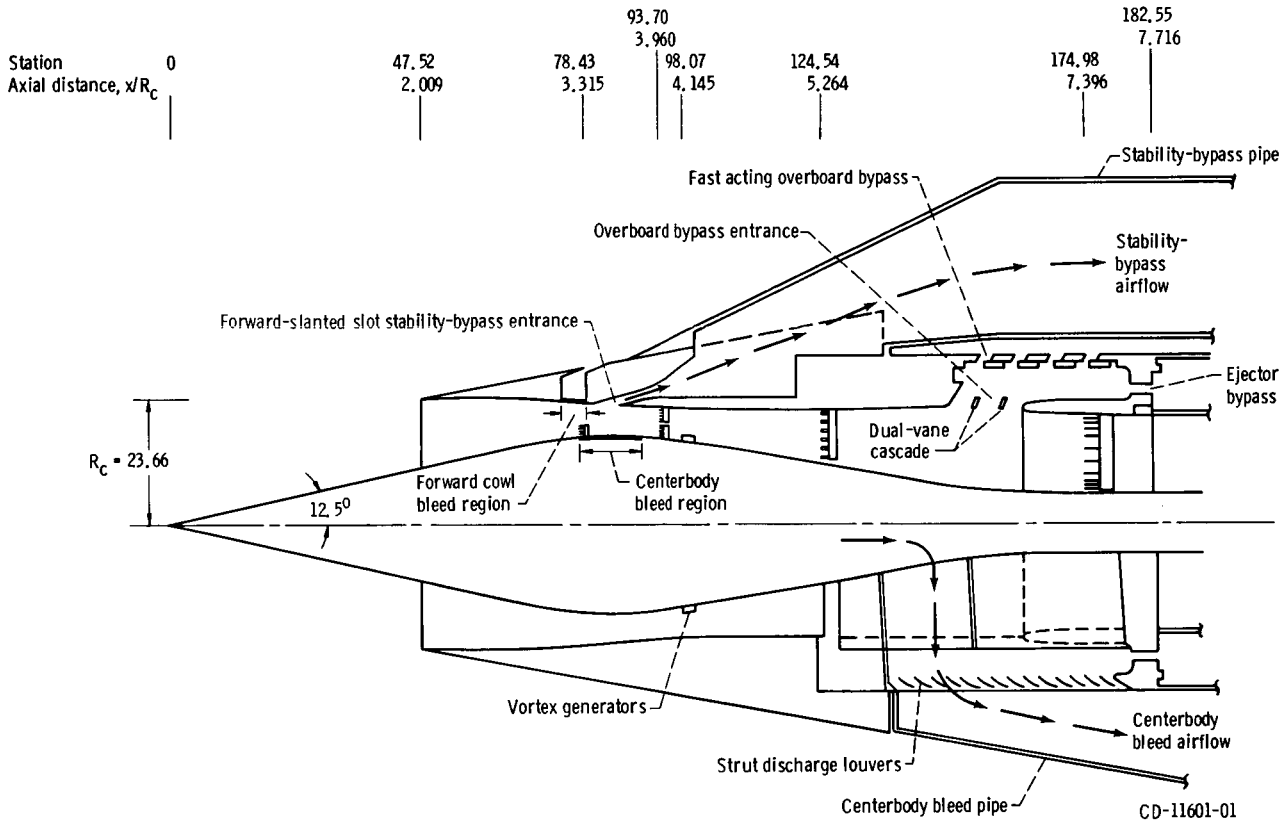

Figure 3. - Inlet details. (All linear dimensions are in cm.)

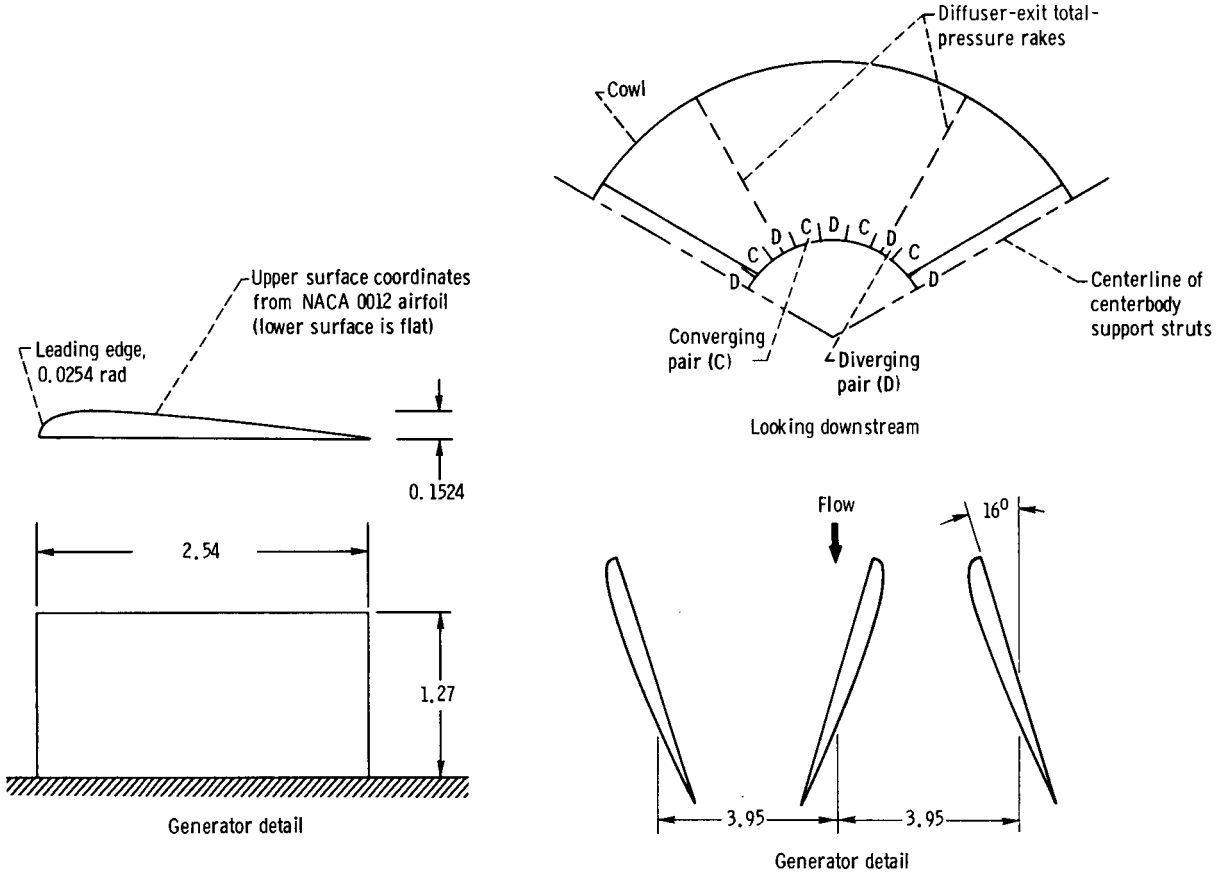

Figure 4. - Vortex generator design. (All linear dimensions are in cm.)

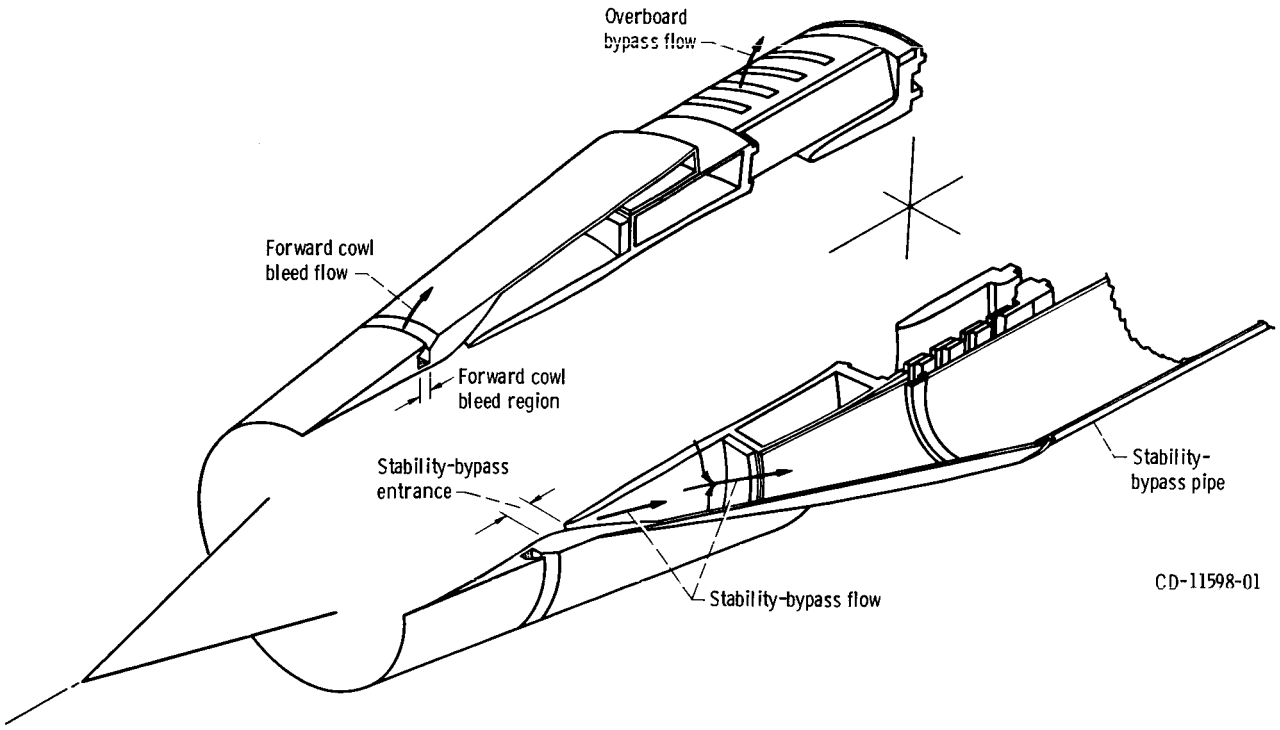

Figure 5. - Sketch of inlet cowl showing cowl bleed and bypass ducting.

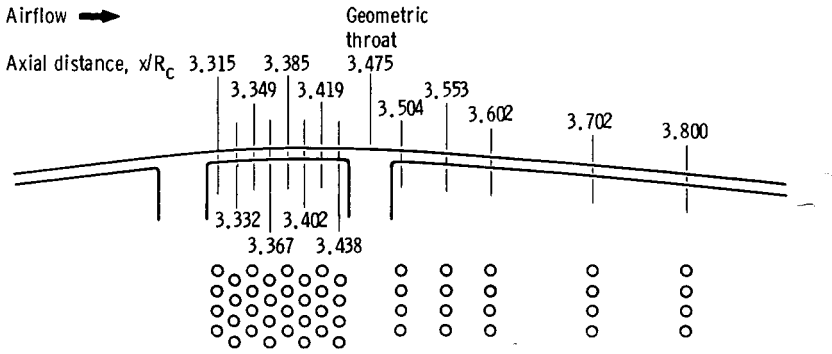

Figure 6. - Centerbody bleed arrangement. Hole diameter, 0.3175 centimeter.

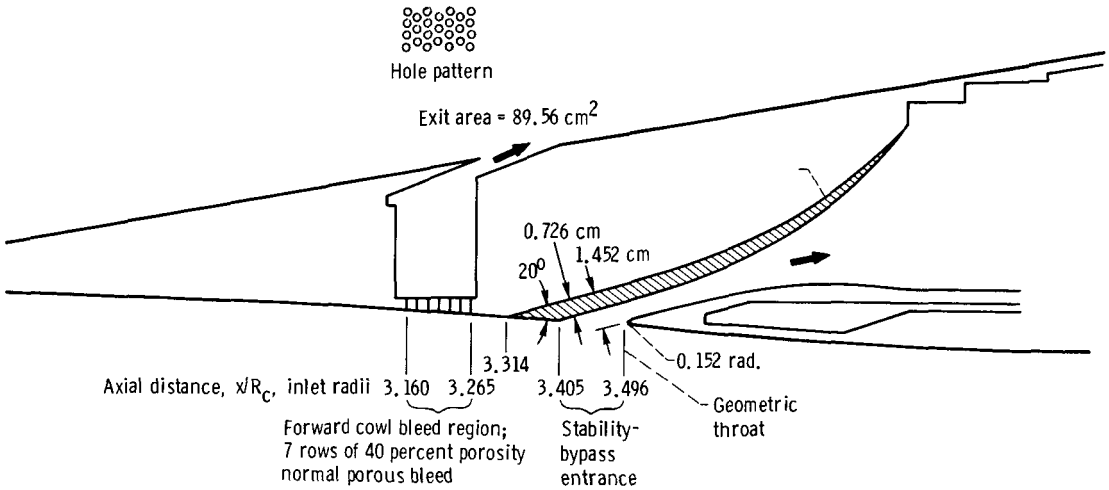

Figure 7. - Forward-slanted slot stability-bypass entrance.

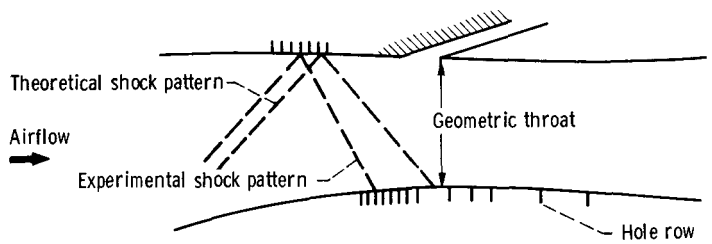

Configuration	Forward cowl bleed region	Forward-slanted slot stability-bypass entrance	Centerbody bleed region
LS	●●●●○○●	Large	○○○○○○●● ●●● ●●
SS	●●●●○○●	Small	○○○○○○●● ●●● ●●

○ Row open ● Row closed

Figure 8. - Inlet stability-bypass entrance and bleed region configurations.

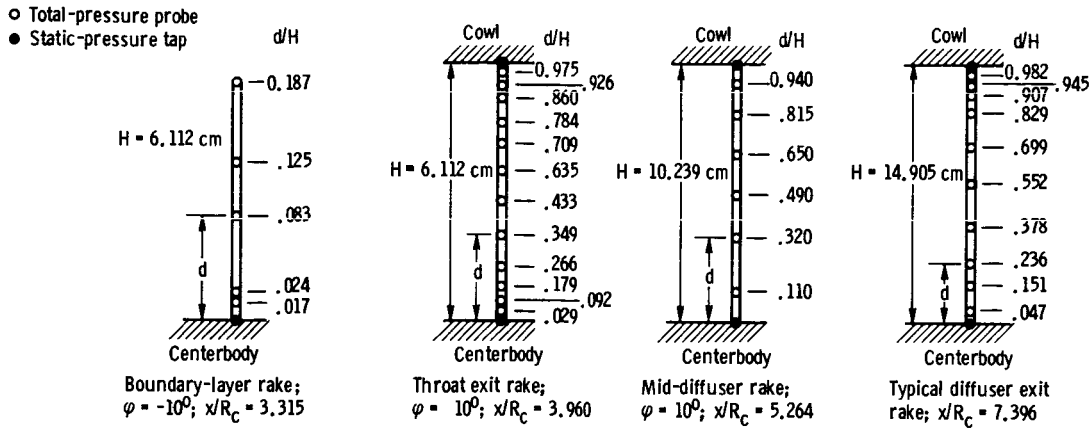

(a) Inlet-total-pressure rake dimensions.

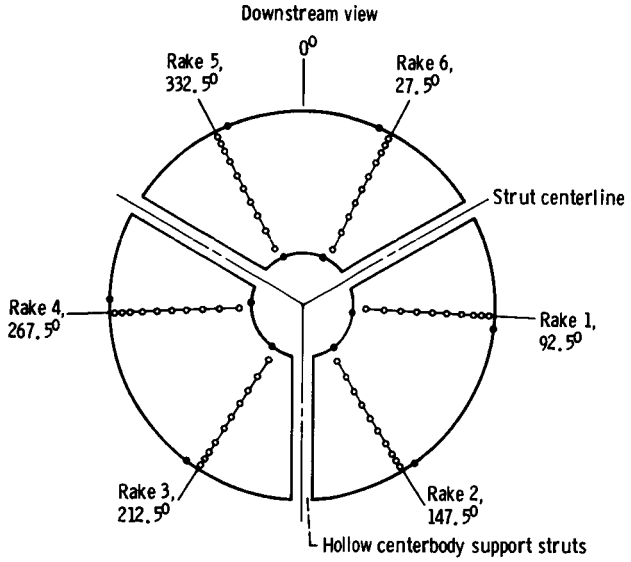

(b) Total- and static-pressure instrumentation at diffuser-exit station, $x/R_c = 7.396$.

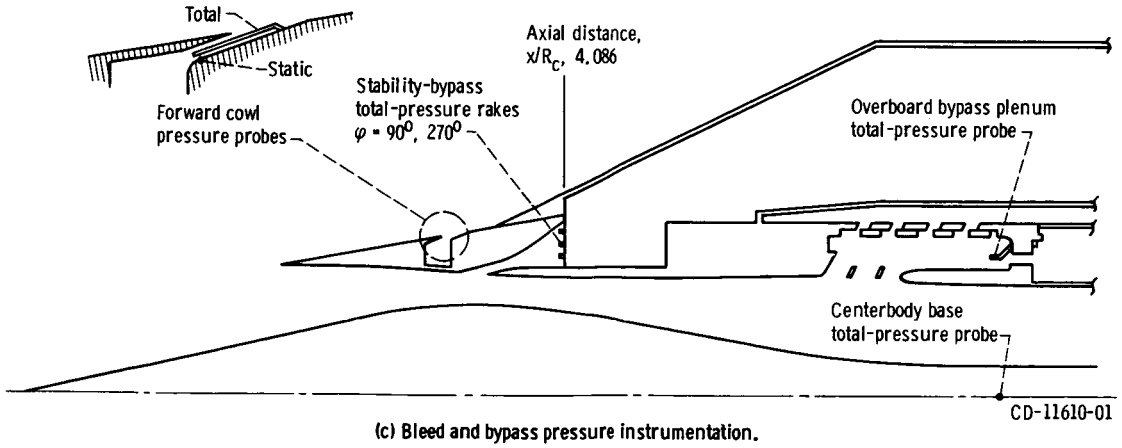

(c) Bleed and bypass pressure instrumentation.

Figure 9. - Inlet-pressure instrumentation (x/R_c is the axial distance from cone tip, φ is the circumferential position, and d/H is the ratio of distance from surface to annulus height).

Slot static-pressure tap locations along top centerline

Tap	L/R_c	Tap	L/R_c
1	-0.015	8	0.246
2	.015	9	.304
3	.055	10	.402
4	.093	11	.485
5	.130	12	.569
6	.164	13	.264
7	.205		

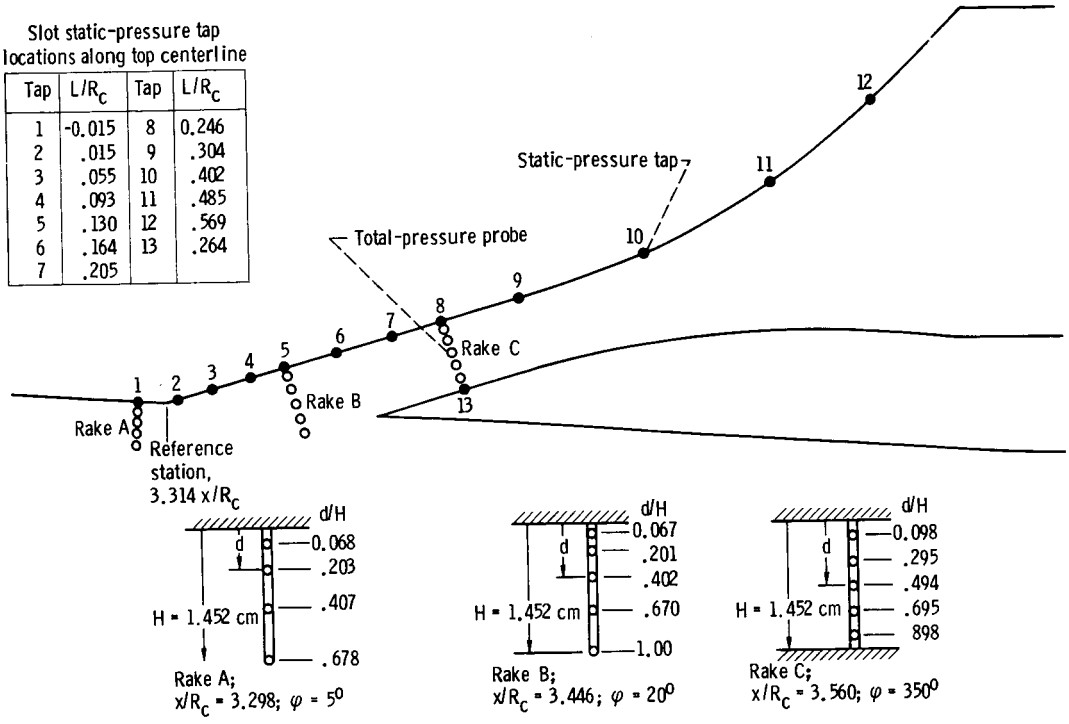

(a) Large forward-slanted slot.

Slot static-pressure tap locations along top centerline

Tap	L/R_c	Tap	L/R_c
1	-0.106	8	0.168
2	-.062	9	.228
3	-.016	10	.308
4	.016	11	.390
5	.061	12	.478
6	.087	13	.173
7	.127		

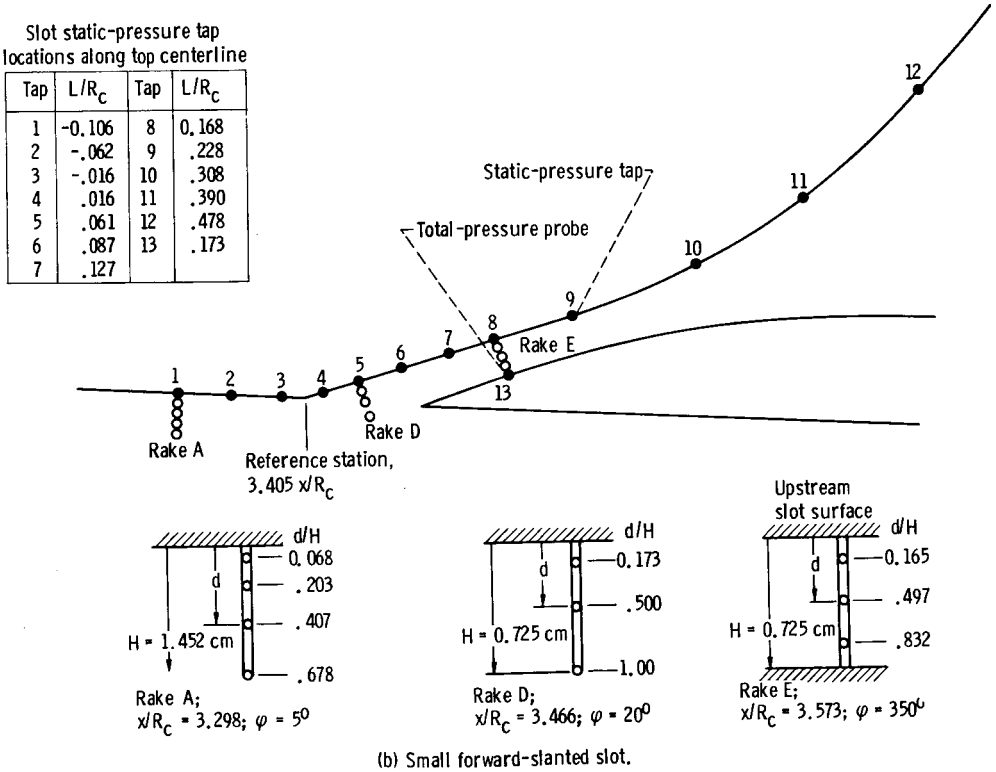

(b) Small forward-slanted slot.

Figure 10. - Forward-slanted-slot pressure instrumentation (wherein x/R_c is the axial position, φ is the circumferential position, d/H is the ratio of distance from surface to annulus height, and L/R_c is the axial distance from reference station.

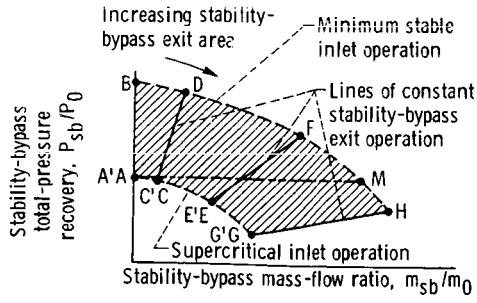

(a) Stability-bypass performance.

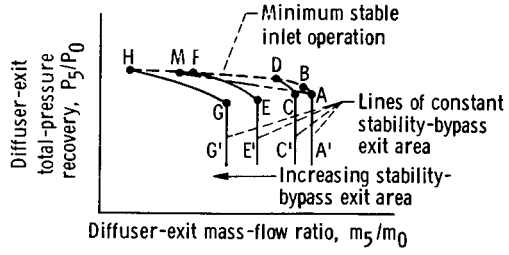

(b) Inlet performance.

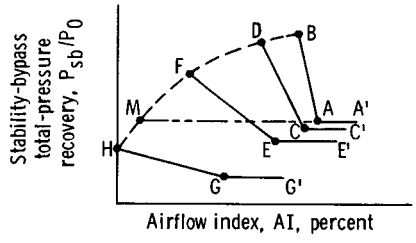

(c) Airflow index.

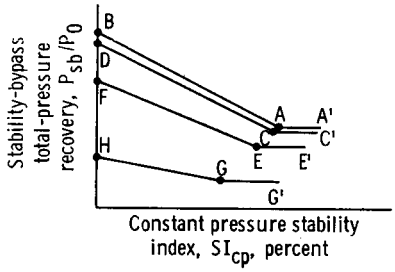

(d) Stability index for constant stability-bypass recovery.

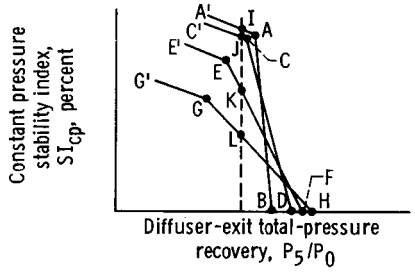

(e) Variation of constant pressure stability index with diffuser-exit total-pressure recovery.

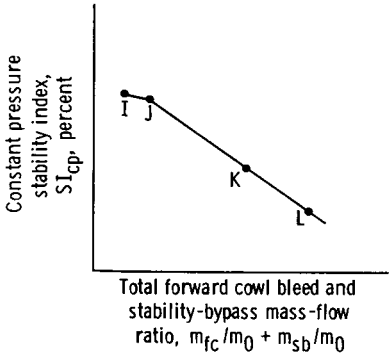

(f) Constant pressure stability index for chosen inlet total-pressure recovery.

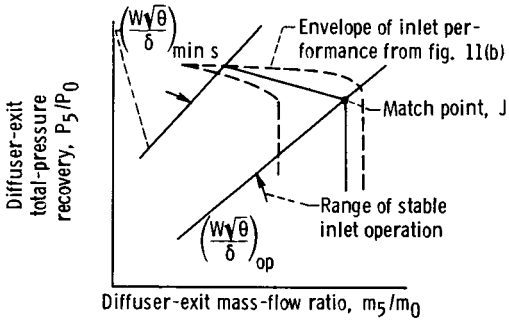

(g) Inlet performance for point J as match condition and with constant pressure bypass-exit control on stability-bypass airflow.

Figure 11. - Inlet stability data.

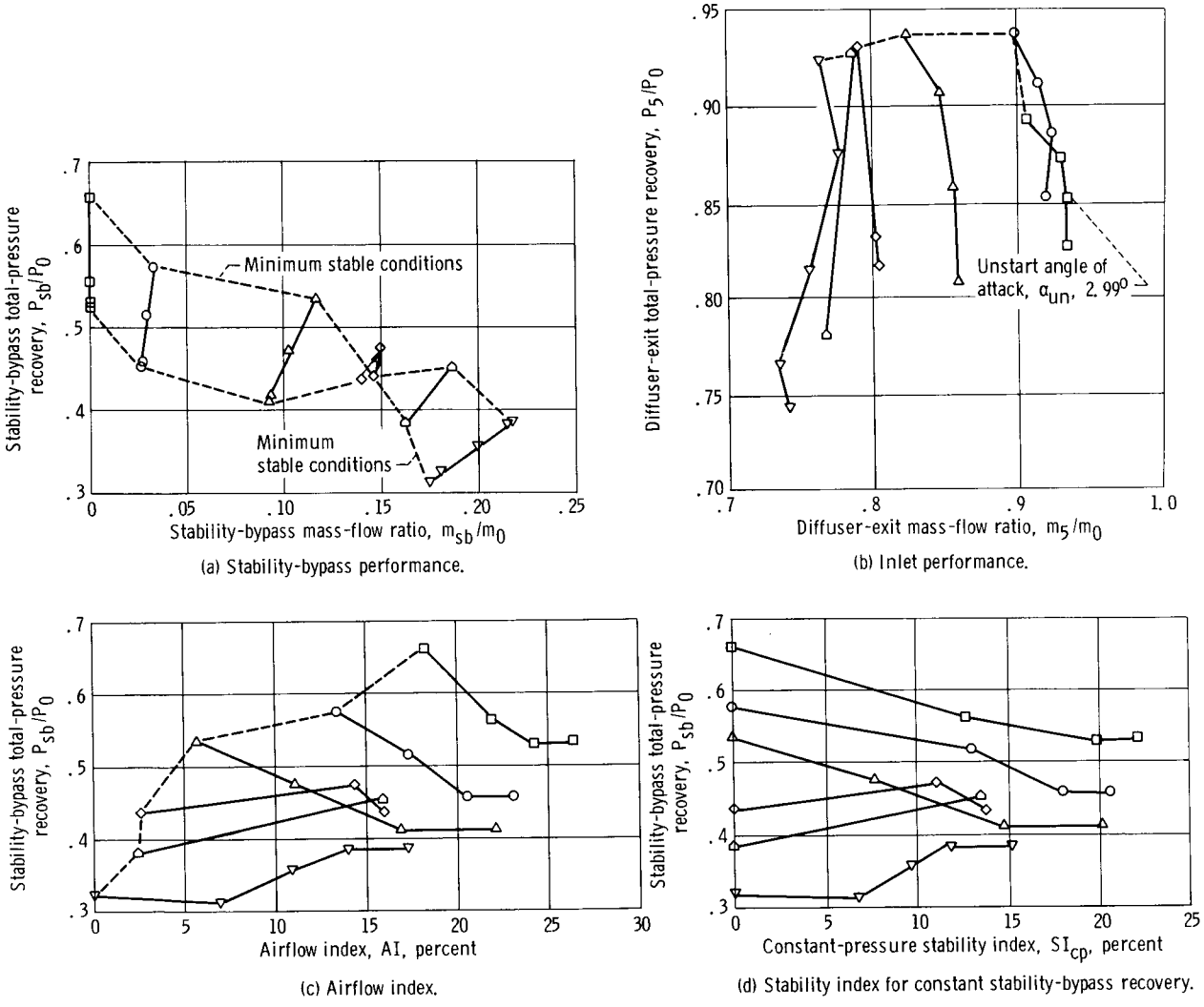

Figure 12. - Performance of large forward-slanted slot configuration LS. Free-stream Mach number, 2.50; angle of attack, 0°; overboard-bypass mass-flow ratio, 0.01.

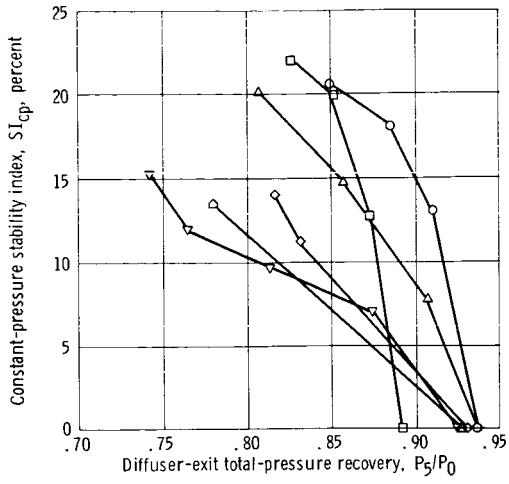

(e) Variation of constant-pressure stability index with diffuser-exit total-pressure recovery.

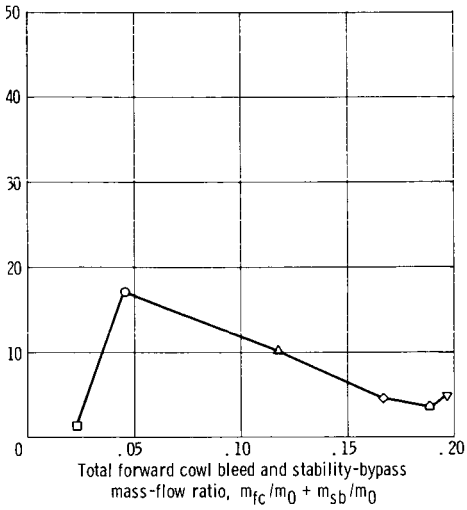

(f) Constant-pressure stability index for an initial diffuser-exit total-pressure recovery of 0.89.

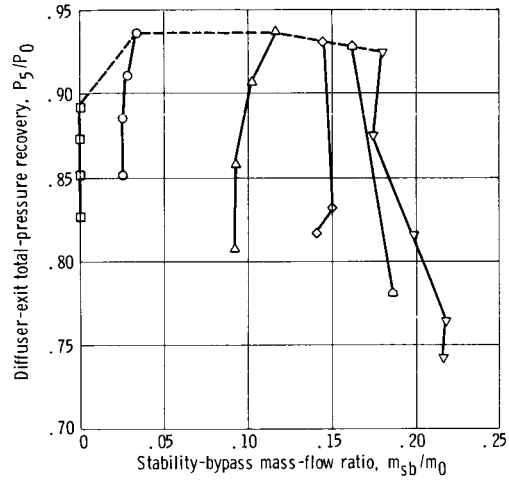

(g) Variation of diffuser-exit total-pressure recovery with stability-bypass mass flow.

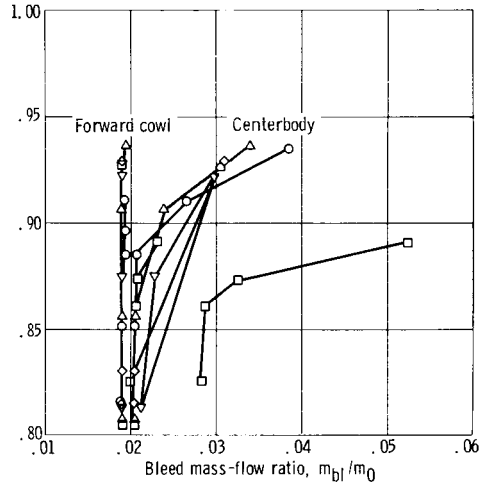

(h) Forward cowl and centerbody bleed performance.

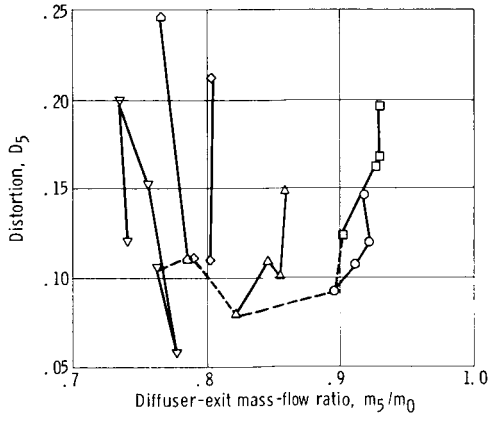

(i) Distortion.

Figure 12. - Concluded.

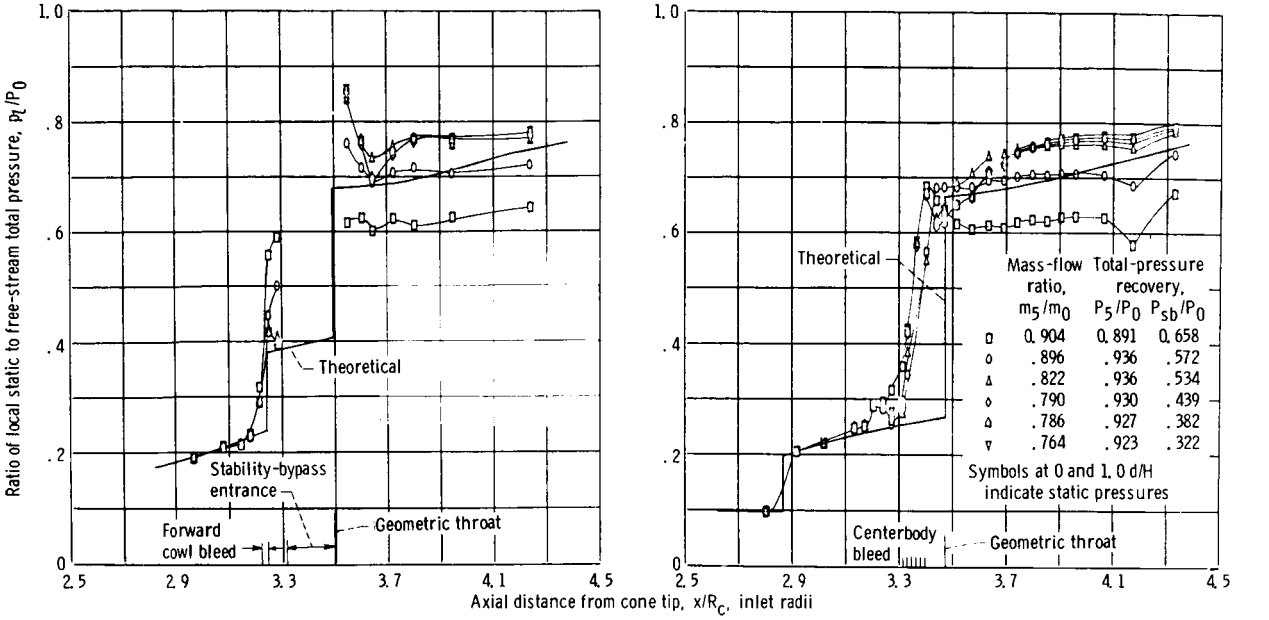

(a) Internal cowl surface pressure distributions.

(b) Centerbody surface pressure distributions.

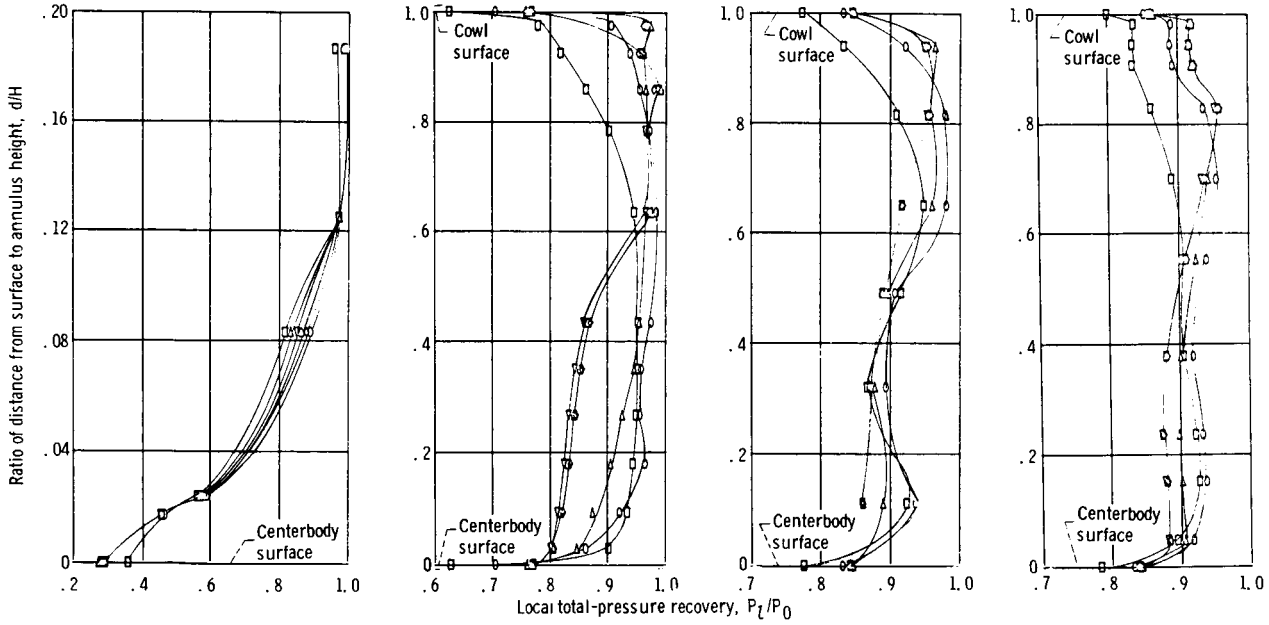

(c) Boundary-layer rake profiles.

(d) Throat-exit rake profiles.

(e) Mid-diffuser rake profiles.

(f) Typical diffuser-exit rake profiles.

Figure 13. - Diffuser static- and total-pressure distributions for configuration LS at minimum stable operation.

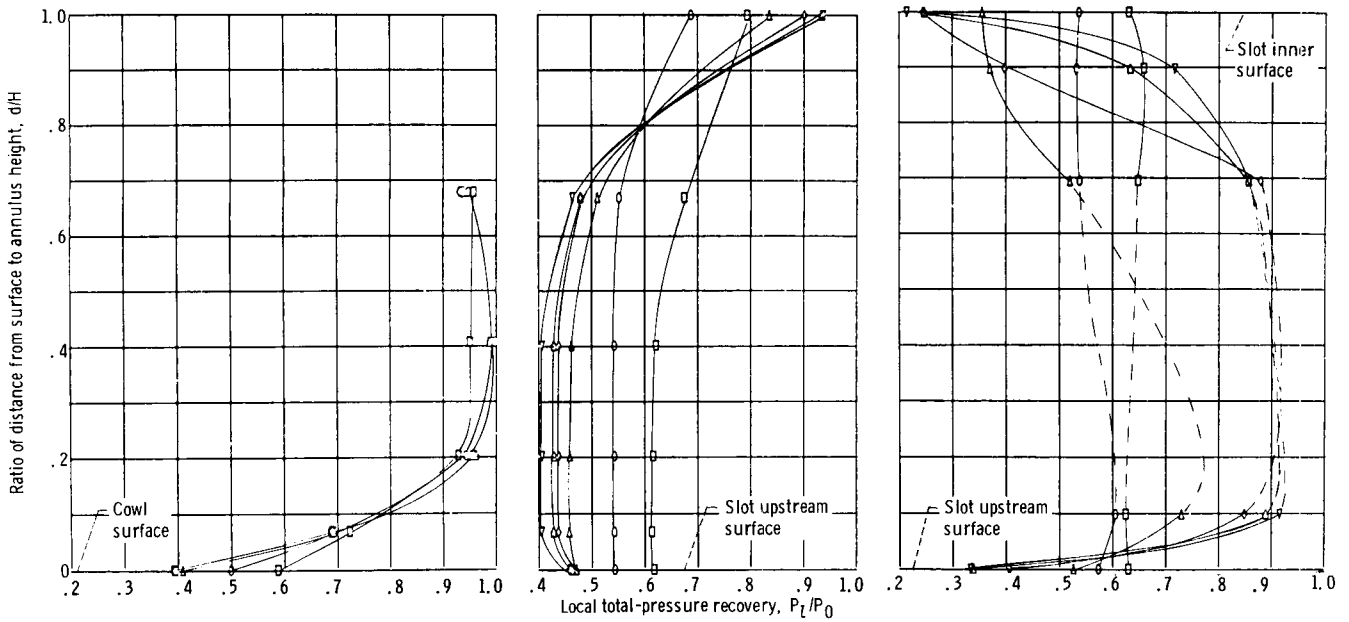

(g) Slot rake A profiles.

(h) Slot rake B profiles.

(i) Slot rake C profiles.

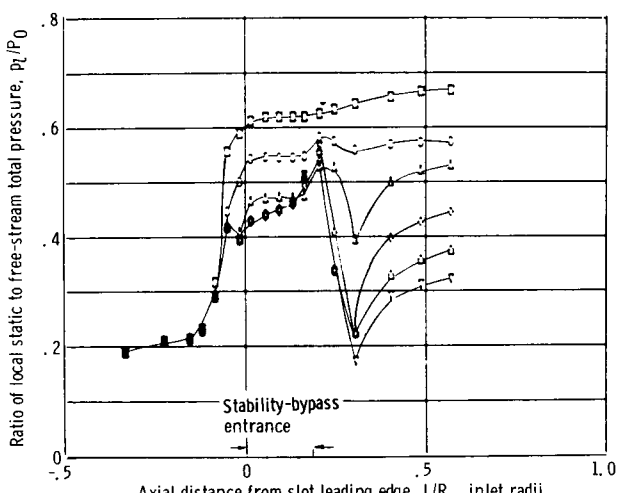

(j) Surface pressure distributions on upstream surface of forward-slanted slot.

	Mass-flow ratio, m_5/m_0	Total-pressure recovery, P_5/P_0	P_{sb}/P_0
□	0.904	0.891	0.658
○	.896	.936	.572
△	.822	.936	.534
◇	.790	.930	.439
▷	.786	.927	.382
▽	.764	.923	.322

Symbols at 0 and 1.0 d/H indicate static pressures

Figure 13. - Concluded.

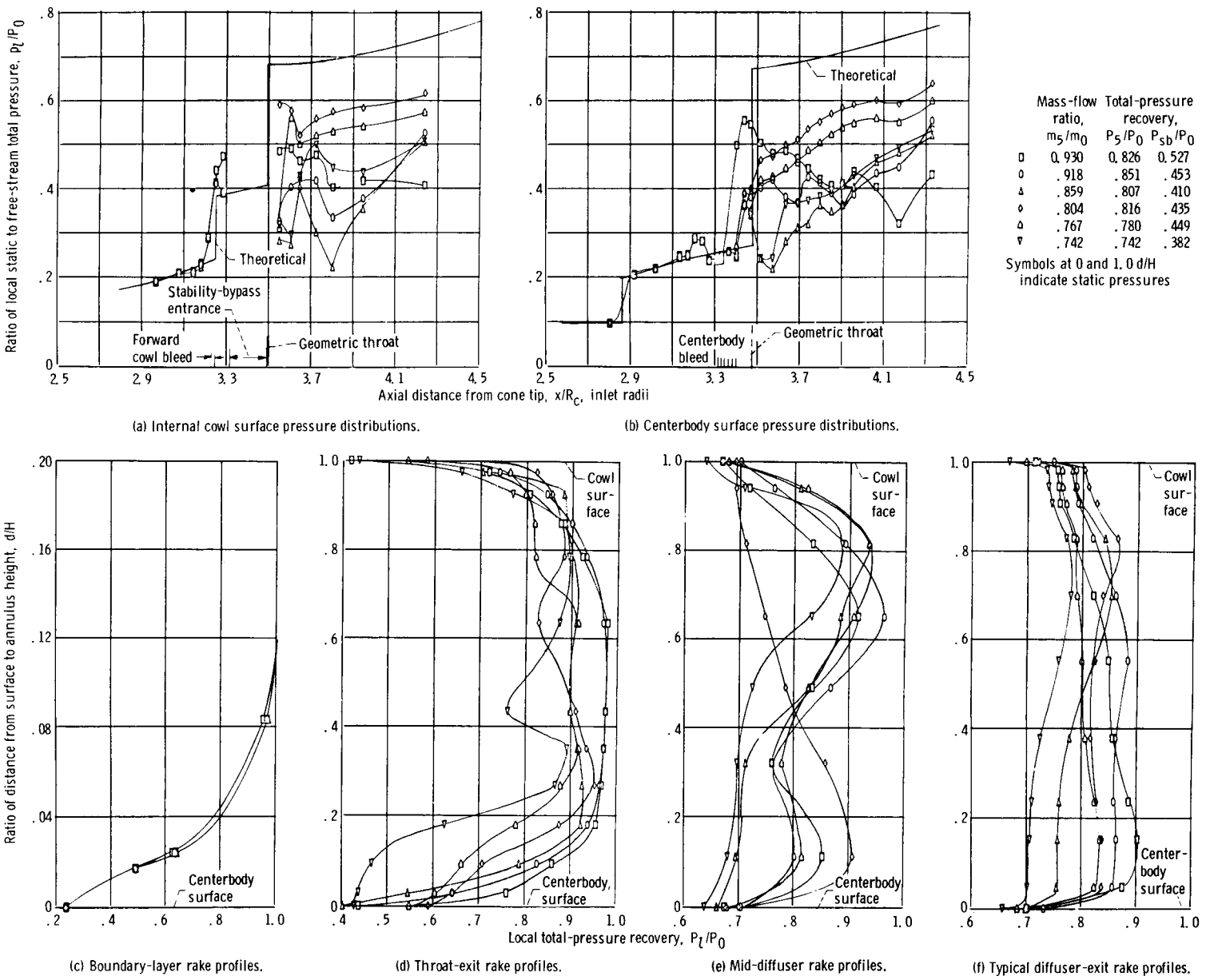

(a) Internal cowl surface pressure distributions.

(b) Centerbody surface pressure distributions.

(c) Boundary-layer rake profiles.

(d) Throat-exit rake profiles.

(e) Mid-diffuser rake profiles.

(f) Typical diffuser-exit rake profiles.

Figure 14 - Diffuser static- and total-pressure distributions for configuration LS at supercritical operation

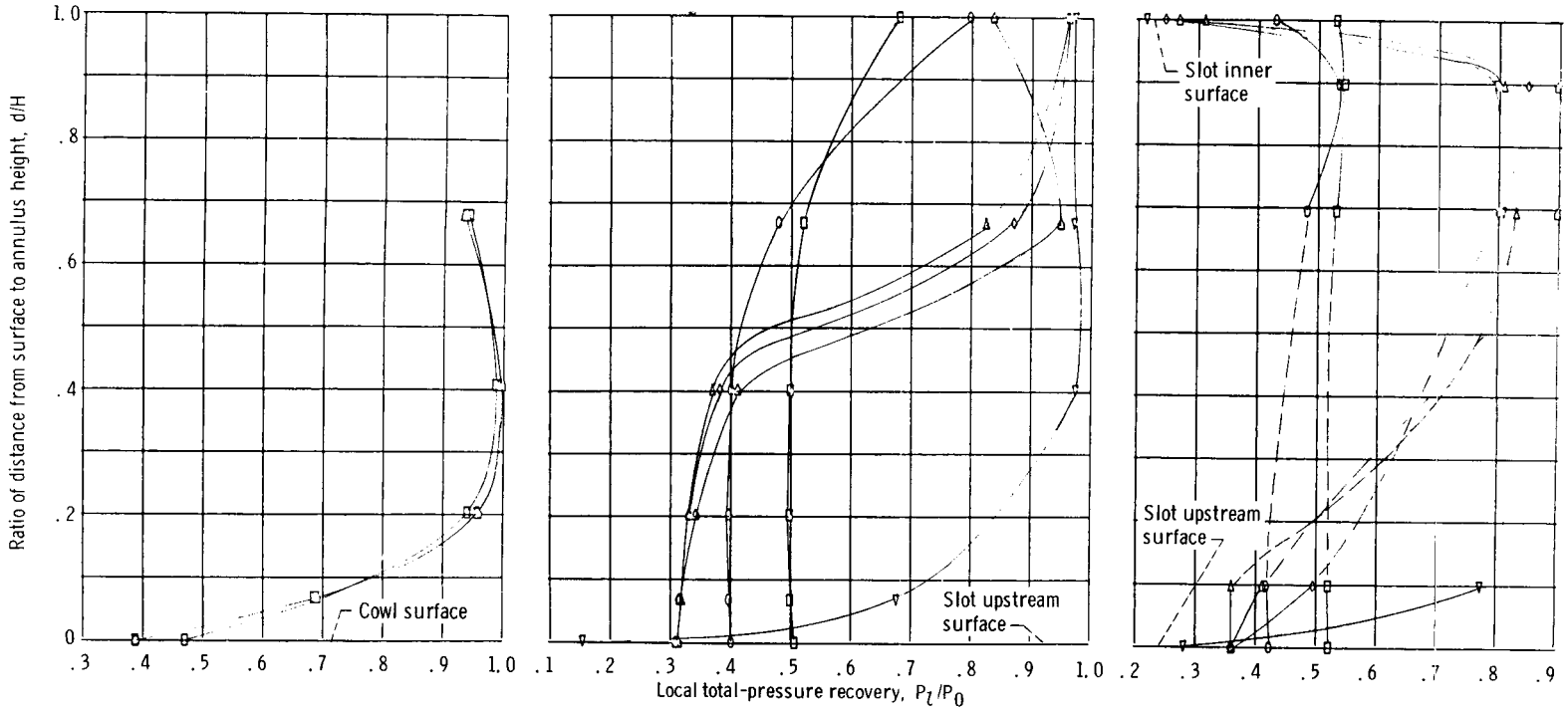

(g) Slot rake A profiles.

(h) Slot rake B profiles.

(i) Slot rake C profiles.

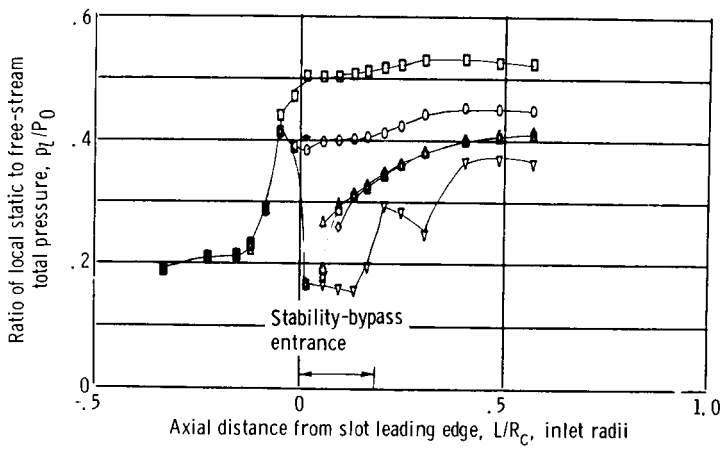

(j) Surface pressure distributions on upstream surface of forward-slanted slot.

	Mass-flow ratio, m_5/m_0	Total-pressure recovery, P_5/P_0	P_{sb}/P_0
□	0.930	0.826	0.527
○	.918	.851	.453
△	.859	.807	.410
◇	.804	.816	.435
⌂	.767	.780	.449
▽	.742	.742	.382

Symbols at 0 and 1.0 d/H indicate static pressures

Figure 14. - Concluded.

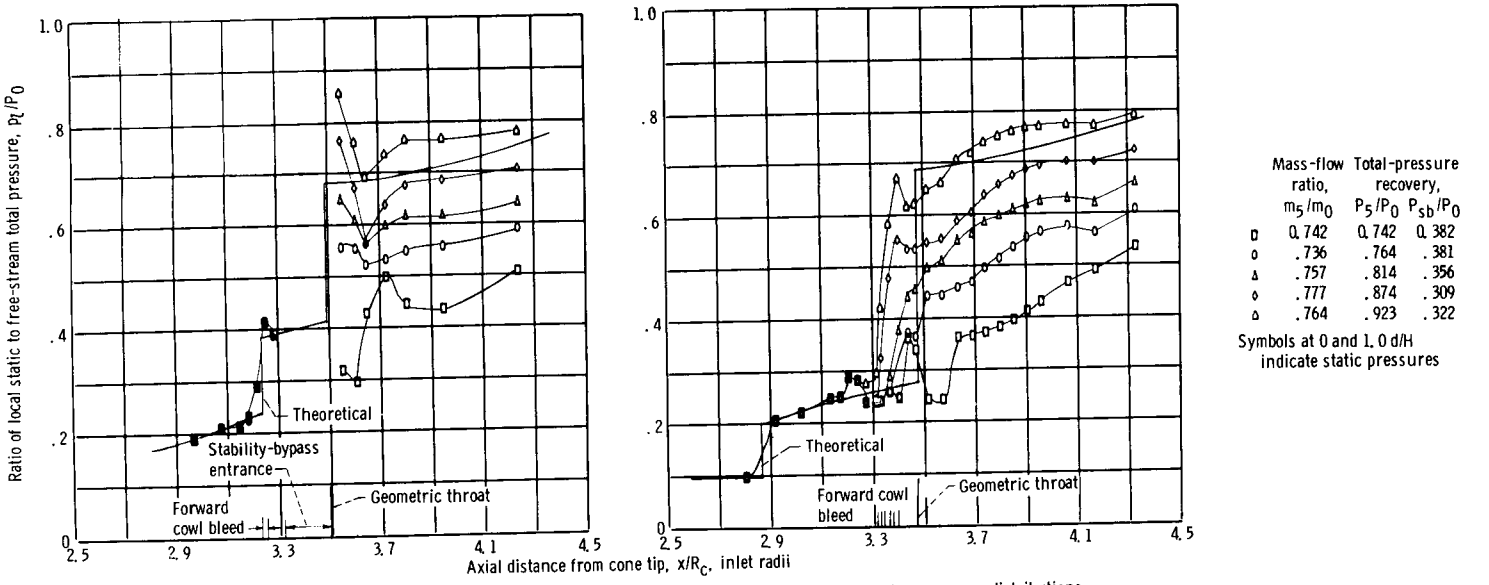

(a) Internal cowl surface pressure distribitions.

(b) Centerbody surface pressure distributions.

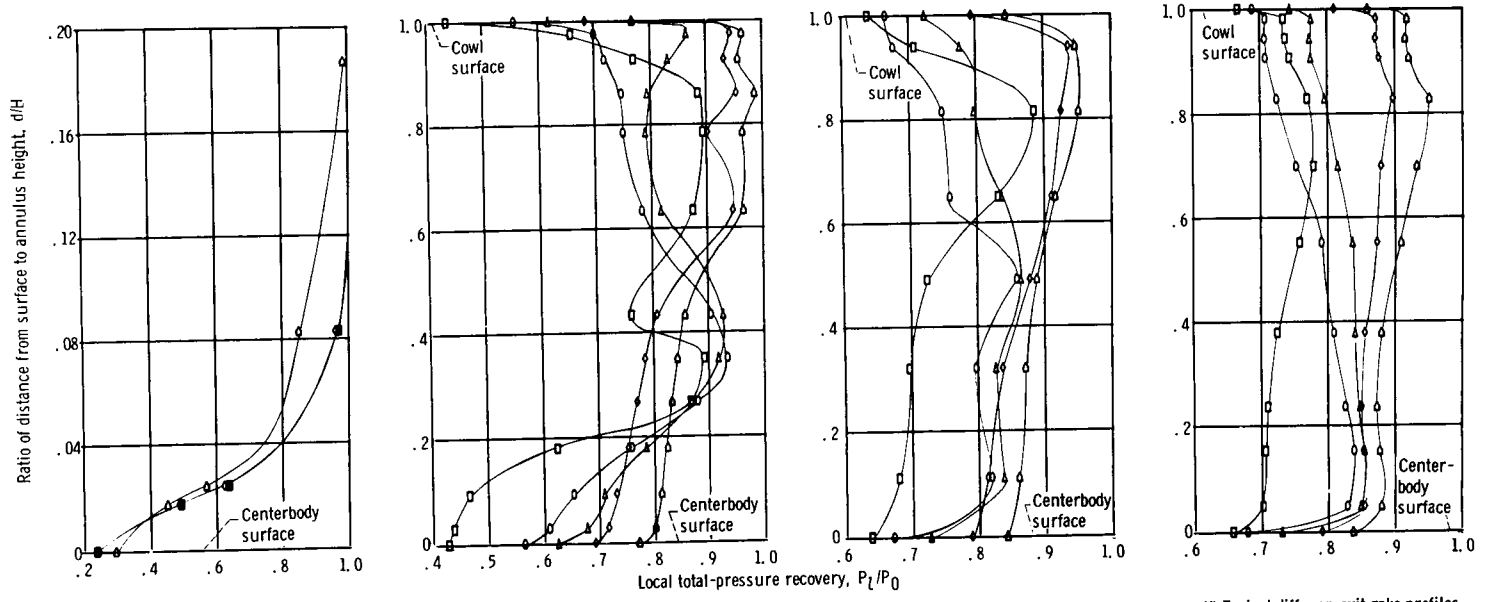

(c) Boundary-layer rake profiles.

(d) Throat-exit rake profiles.

(e) Mid-diffuser rake profiles.

(f) Typical diffuser-exit rake profiles.

Figure 15. - Diffuser static- and total-pressure distributions for configuration LS at largest stability-bypass exit area.

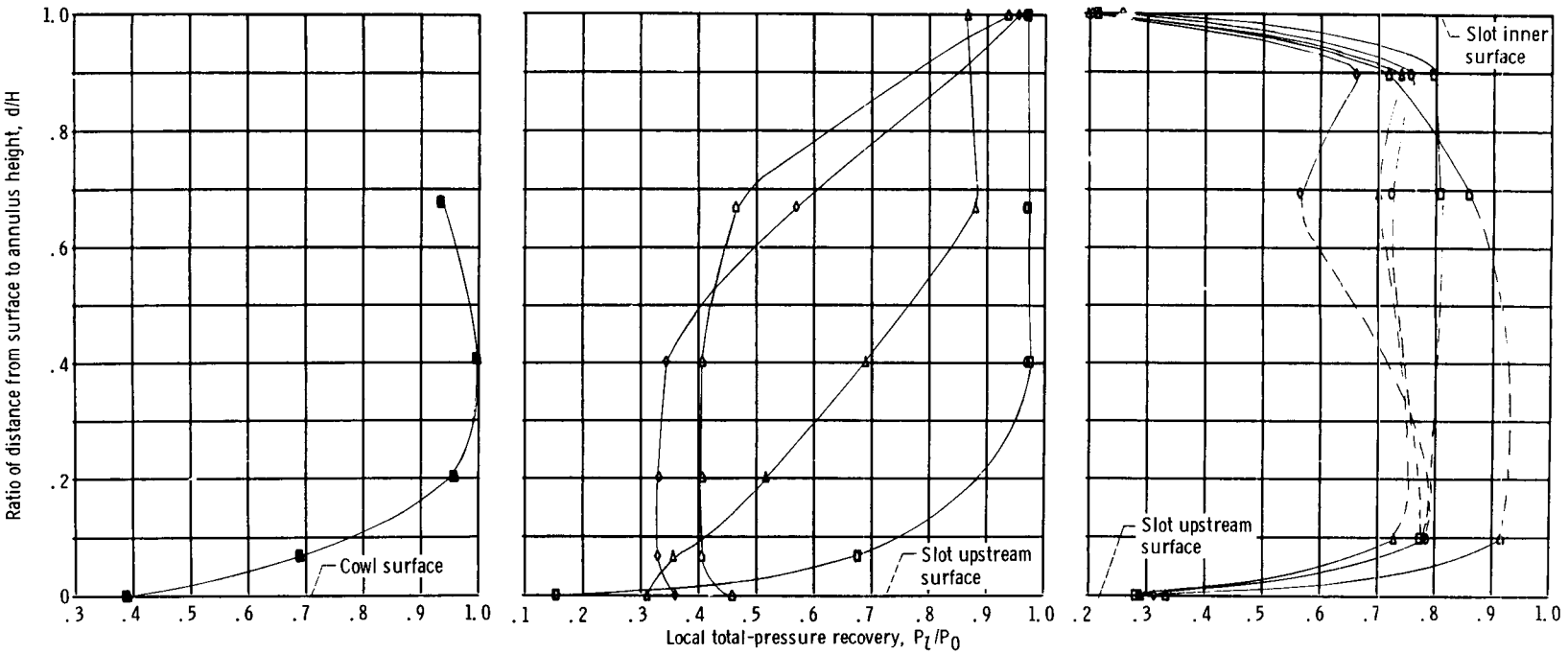

(g) Slot rake A profiles.

(h) Slot rake B profiles.

(i) Slot rake C profiles.

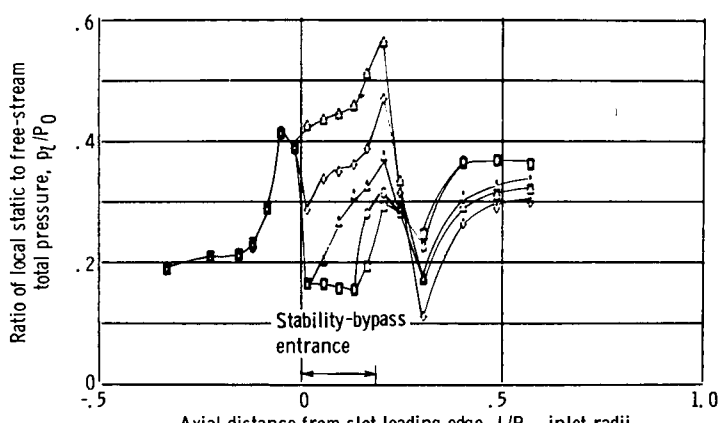

(j) Surface pressure distributions on upstream surface of forward-slanted slot.

	Mass-flow ratio, m_5/m_0	Total-pressure recovery, P_5/P_0	P_{sb}/P_0
□	0.742	0.742	0.382
○	.736	.764	.381
△	.757	.814	.356
◇	.777	.874	.309
▽	.764	.923	.322

Symbols at 0 and 1.0 d/H indicate static pressures

Figure 15. - Concluded.

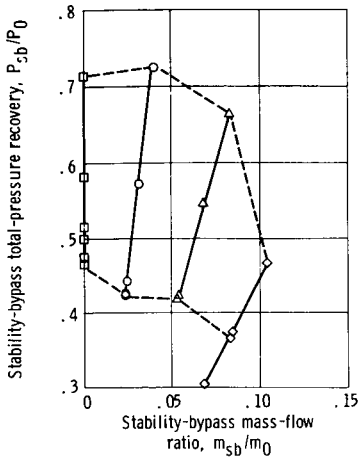

(a) Stability-bypass performance.

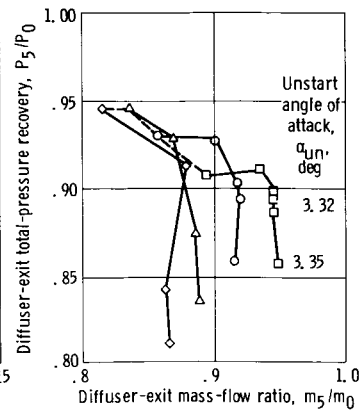

(b) Inlet performance.

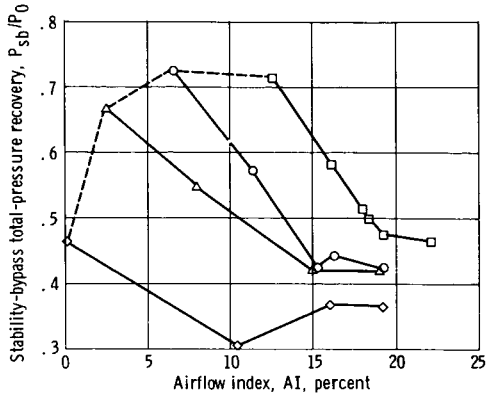

(c) Airflow index.

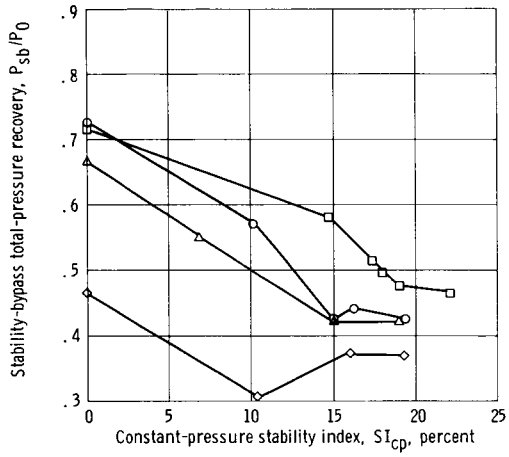

(d) Stability index for constant stability-bypass recovery.

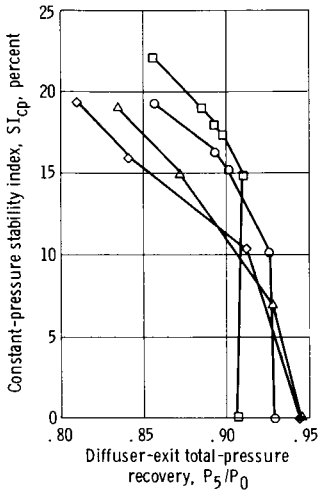

(e) Variation of constant-pressure stability index with diffuser-exit total-pressure recovery.

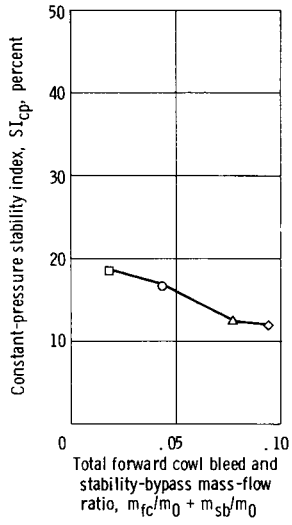

(f) Constant-pressure stability index for an initial diffuser-exit total-pressure recovery of 0.89.

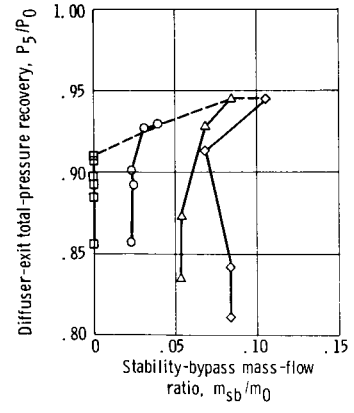

(g) Variation of diffuser-exit total-pressure recovery with stability-bypass recovery.

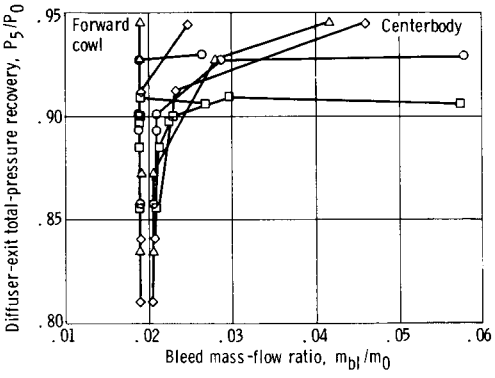

(h) Forward cowl and centerbody bleed performance.

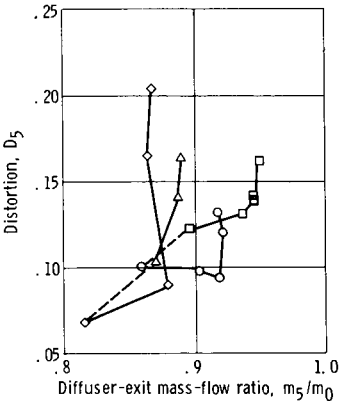

(i) Distortion.

Figure 16. - Performance of small forward-slanted slot configuration SS. Free-stream Mach number, 2.50; angle of attack, 0^0; overboard-bypass mass-flow ratio, 0.01.

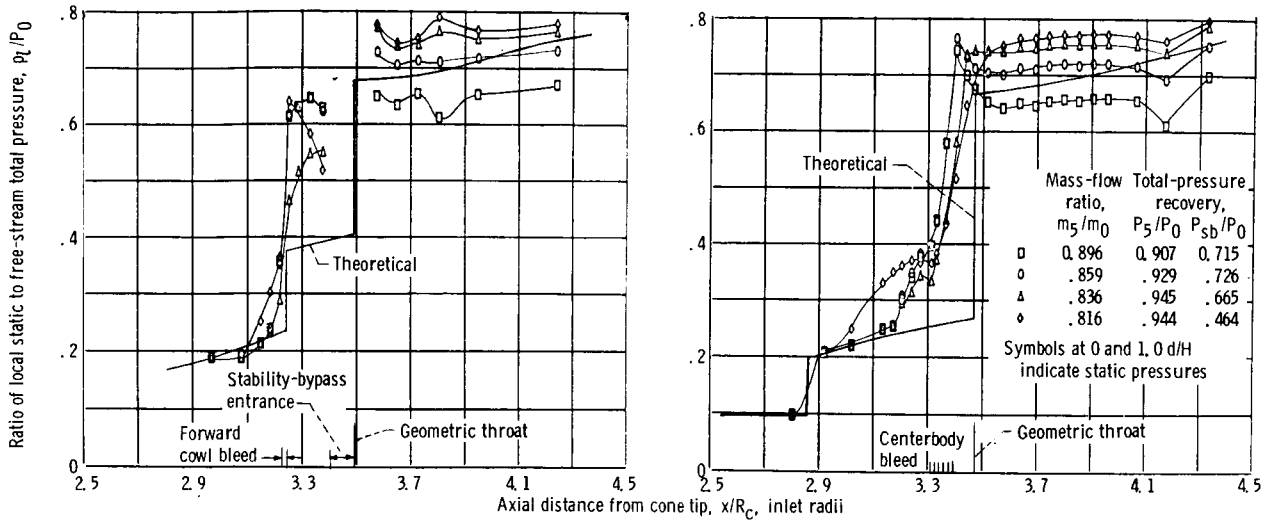

(a) Internal cowl surface pressure distributions.

(b) Centerbody surface pressure distributions.

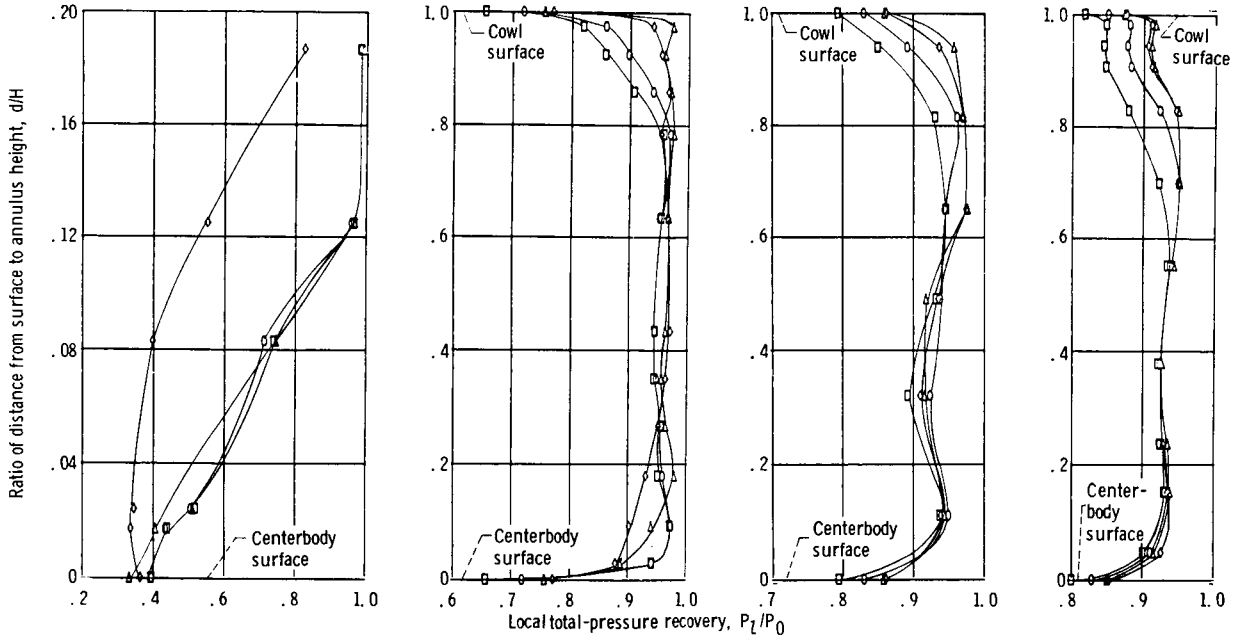

(c) Boundary-layer rake profiles.

(d) Throat-exit rake profiles.

(e) Mid-diffuser rake profiles.

(f) Typical diffuser-exit rake profiles.

Figure 17. - Diffuser static- and total-pressure distributions for configuration SS at minimum stable operation.

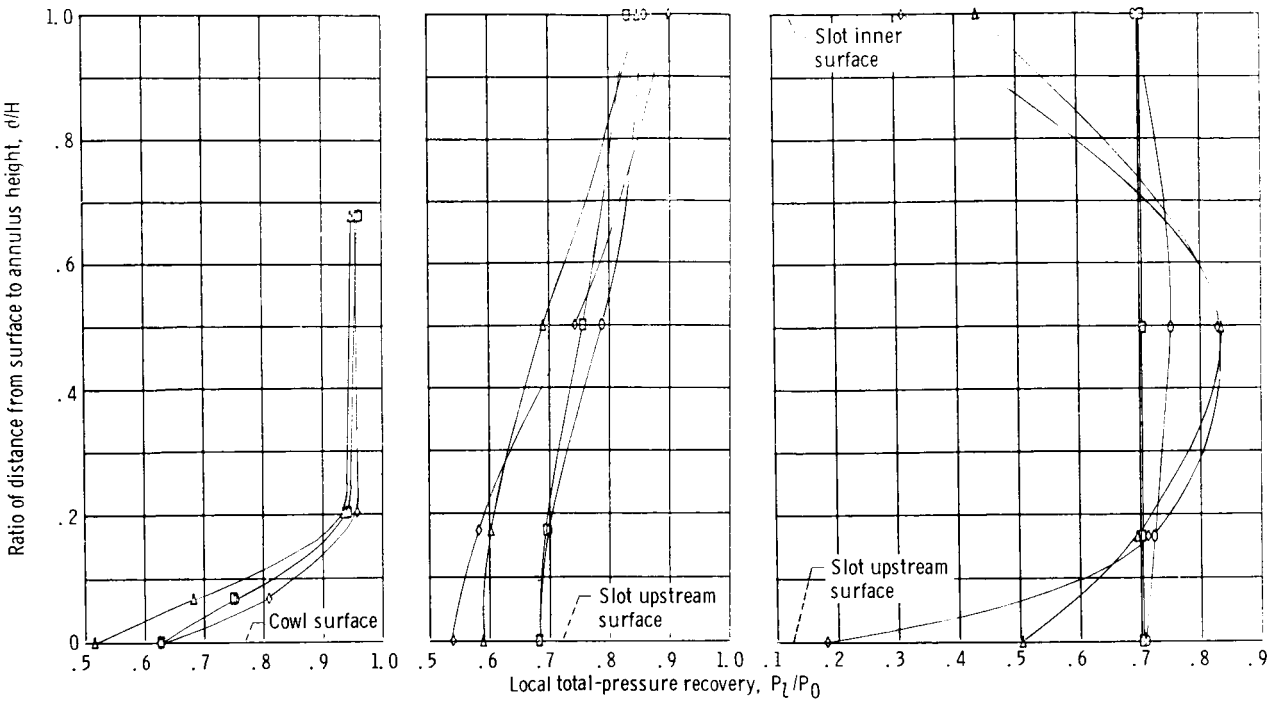

(g) Slot rake A profiles.

(h) Slot rake D profiles.

(i) Slot rake E profiles.

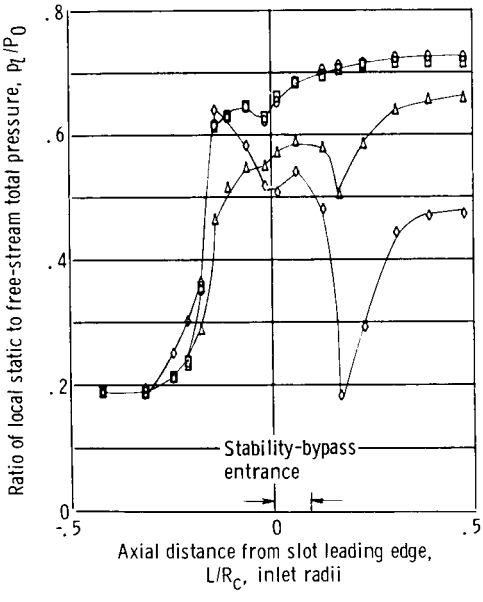

(j) Surface pressure distributions on upstream surface of forward-slanted slot.

	Mass-flow ratio, m_5/m_0	Total-pressure recovery, P_5/P_0	P_{sb}/P_0
□	0.896	0.907	0.715
○	.859	.929	.726
△	.836	.945	.665
◇	.816	.944	.464

Symbols at 0 and 1.0 d/H indicate static pressures

Figure 17. - Concluded.

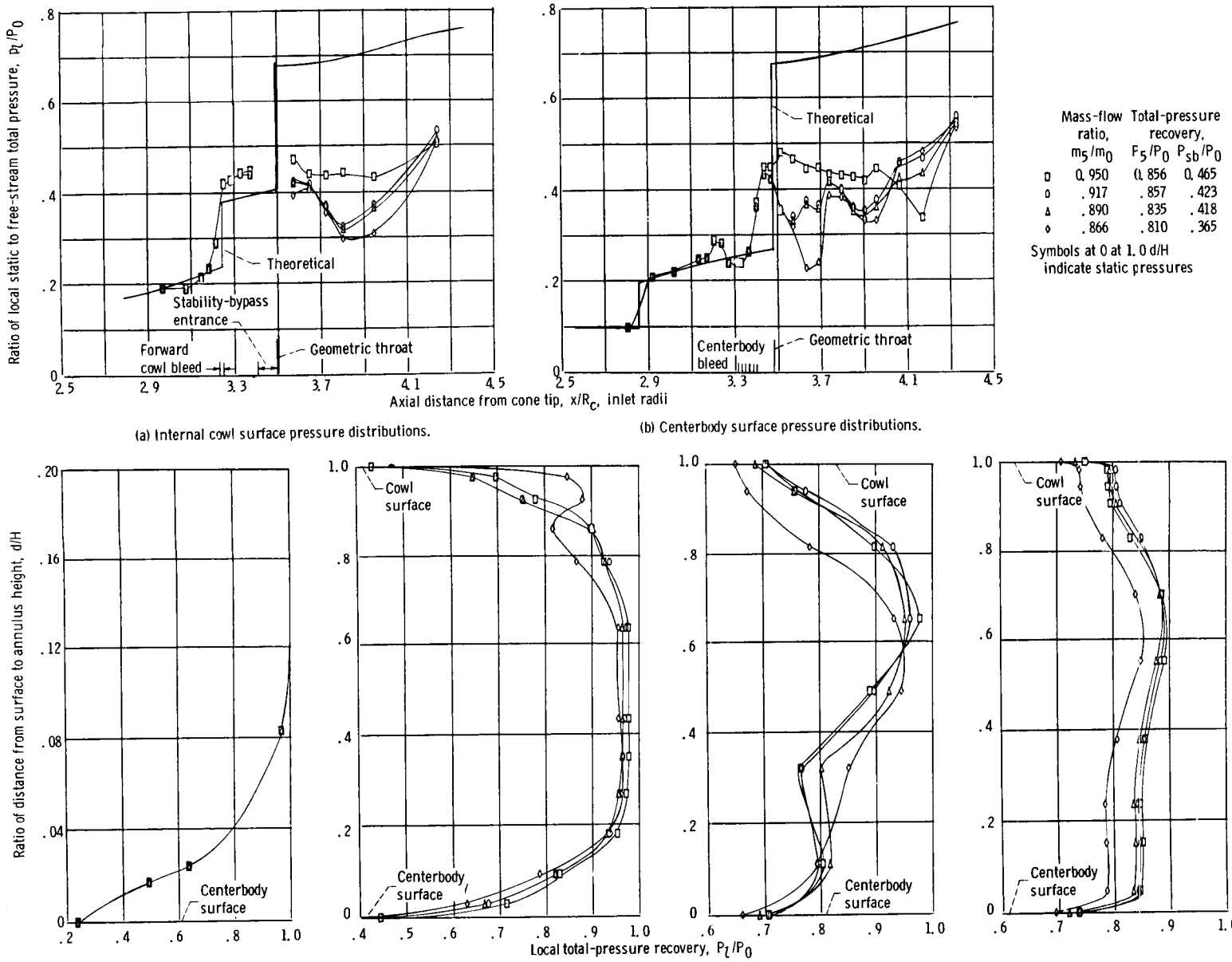

(a) Internal cowl surface pressure distributions.

(b) Centerbody surface pressure distributions.

(c) Boundary-layer rake profiles.

(d) Throat-exit rake profiles.

(e) Mid-diffuser rake profiles.

(f) Typical diffuser-exit rake profiles.

Figure 18. - Diffuser static- and total-pressure distributions for configuration SS at supercritical operation.

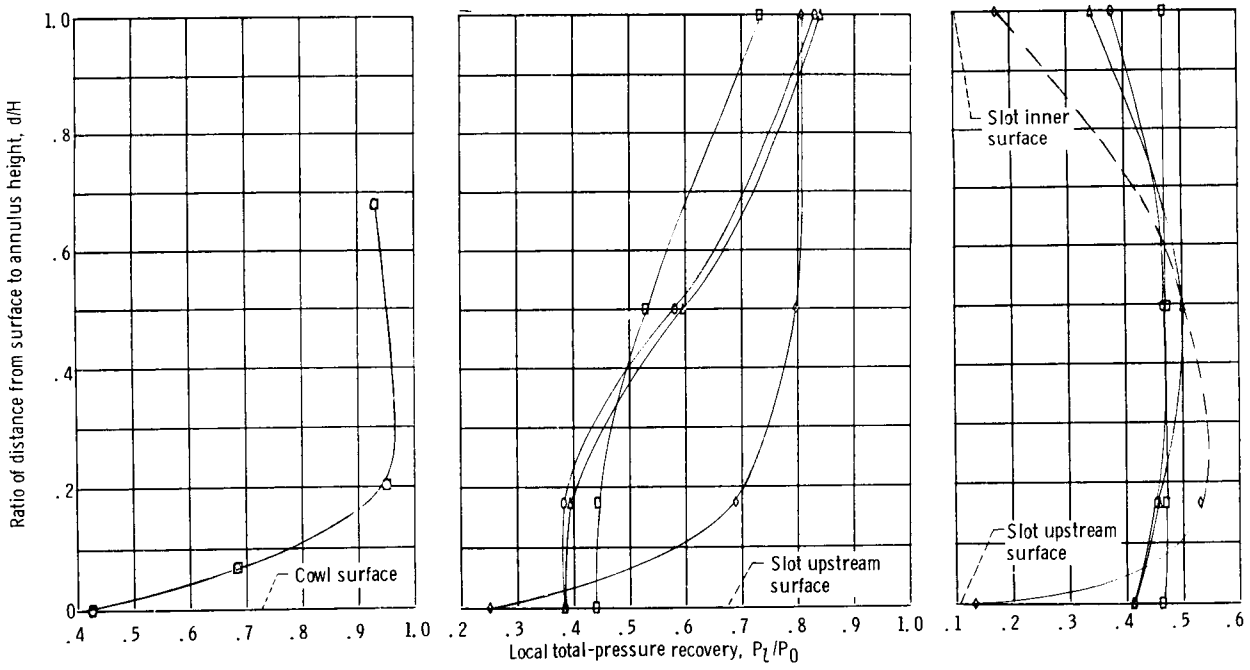

(g) Slot rake A profiles.

(h) Slot rake D profiles.

(i) Slot rake E profiles.

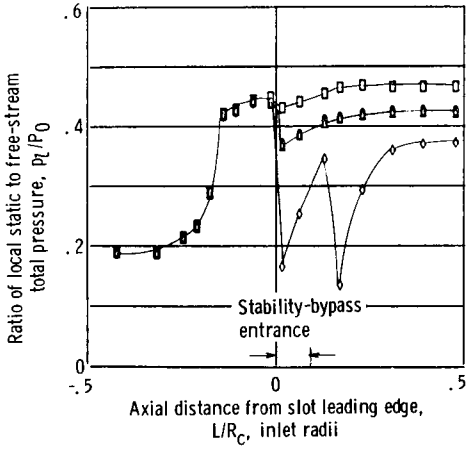

(j) Surface pressure distributions on upstream surface of forward-slanted slot.

	Mass-flow ratio, m_5/m_0	Total-pressure recovery, P_5/P_0	P_{sb}/P_0
□	0.950	0.856	0.465
○	.917	.857	.423
△	.890	.835	.418
◇	.866	.810	.365

Symbols at 0 and 1.0 d/H indicate static pressures

Figure 18. - Concluded.

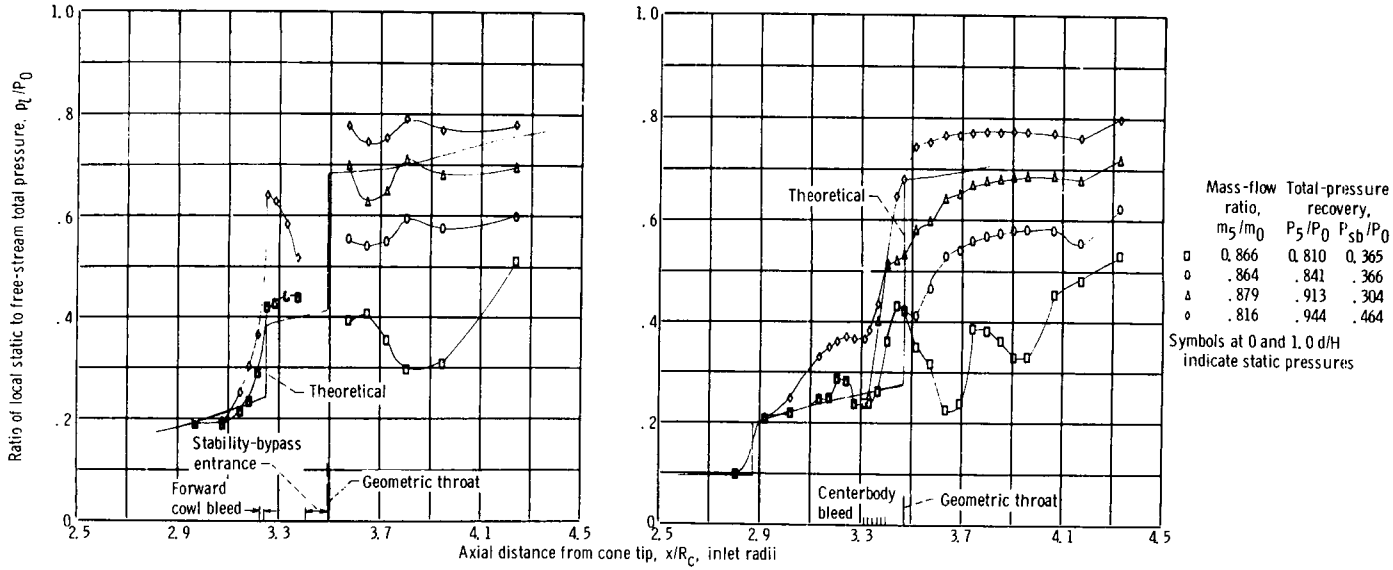

(a) Internal cowl surface pressure distributions.

(b) Centerbody surface pressure distributions.

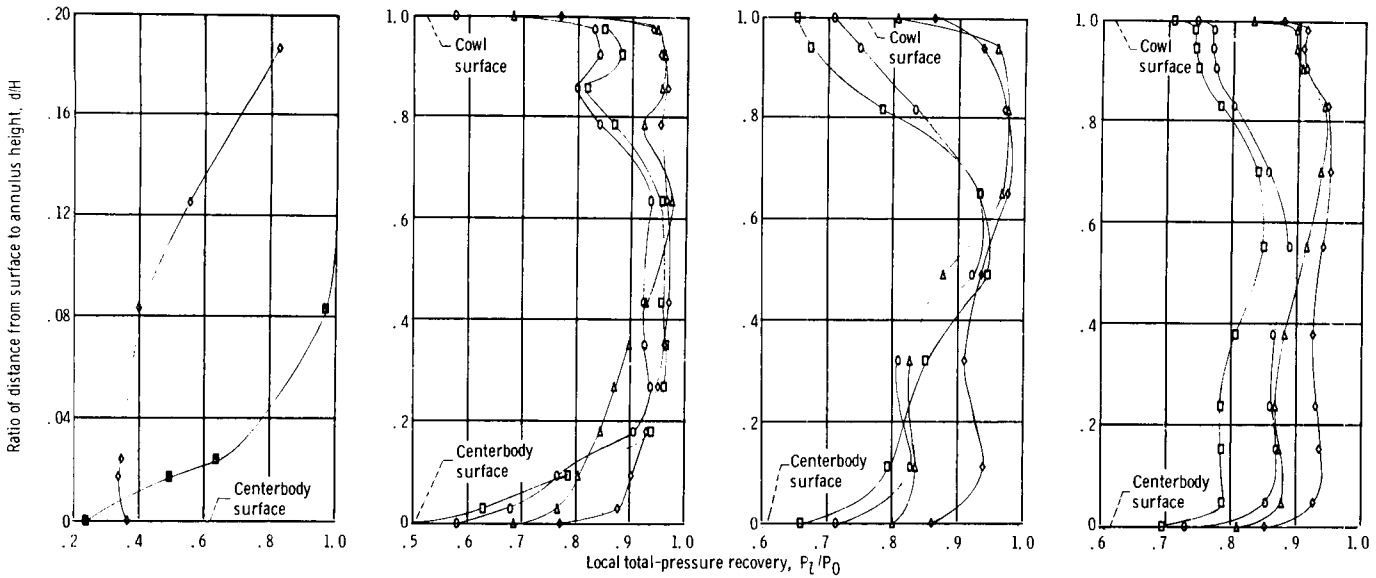

(c) Boundary-layer rake profiles.

(d) Throat-exit rake profiles.

(e) Mid-diffuser rake profiles.

(f) Typical diffuser-exit rake profiles.

Figure 19. - Diffuser static- and total-pressure distributions for configuration SS at largest stability-bypass exit area.

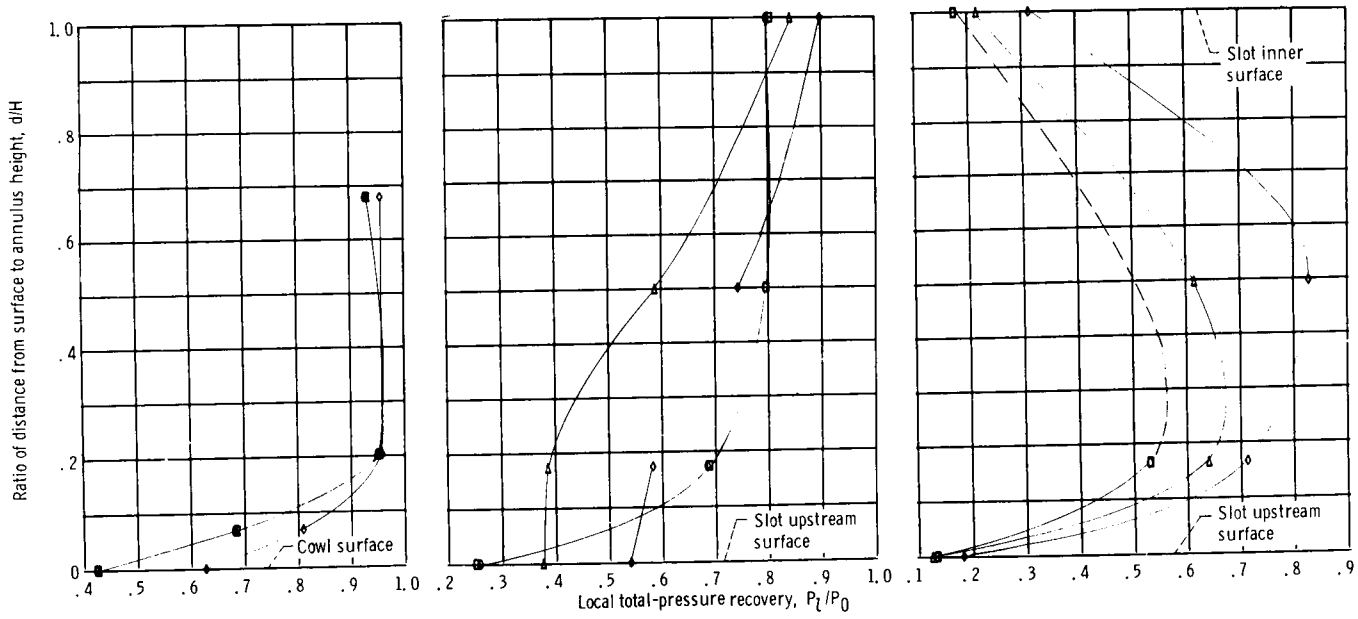

(g) Slot rake A profiles.

(h) Slot rake D profiles.

(i) Slot rake E profiles.

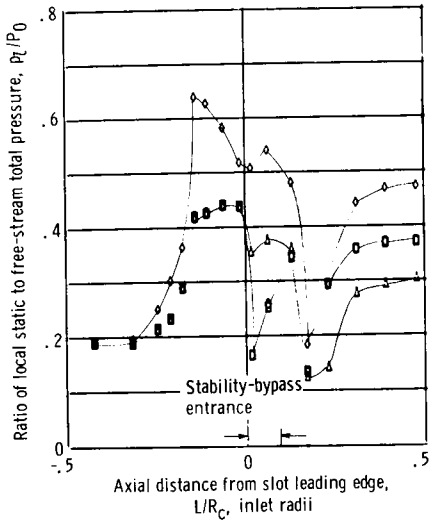

(j) Surface pressure distributions on upstream surface of forward-slanted slot.

	Mass-flow ratio, m_5/m_0	Total-pressure recovery, P_5/P_0	P_{sb}/P_0
□	0.866	0.810	0.365
○	.864	.841	.366
△	.879	.913	.304
◇	.816	.944	.464

Symbols at 0 and 1.0 d/H indicate static pressures

Figure 19. - Concluded.

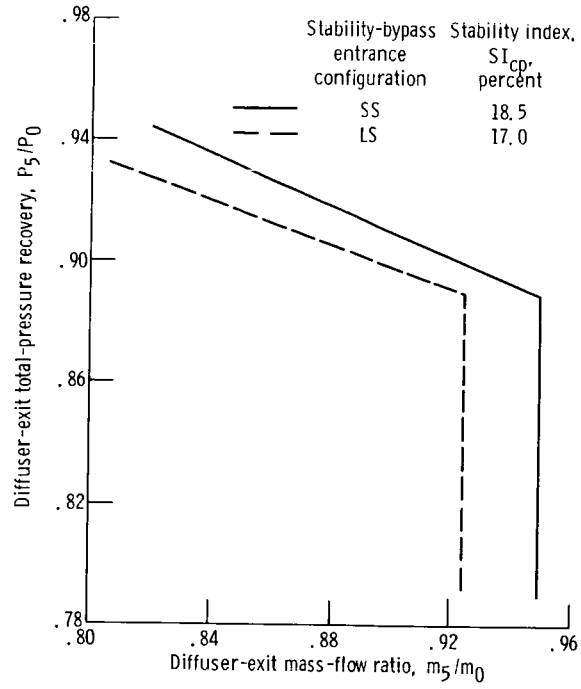

Figure 20. - Comparison of inlet performance based on constant stability-bypass recovery to unstart limit from initial inlet conditions of 89 percent total-pressure recovery. Free-stream Mach number, 2.50; overboard-bypass mass-flow ratio, 0.01.

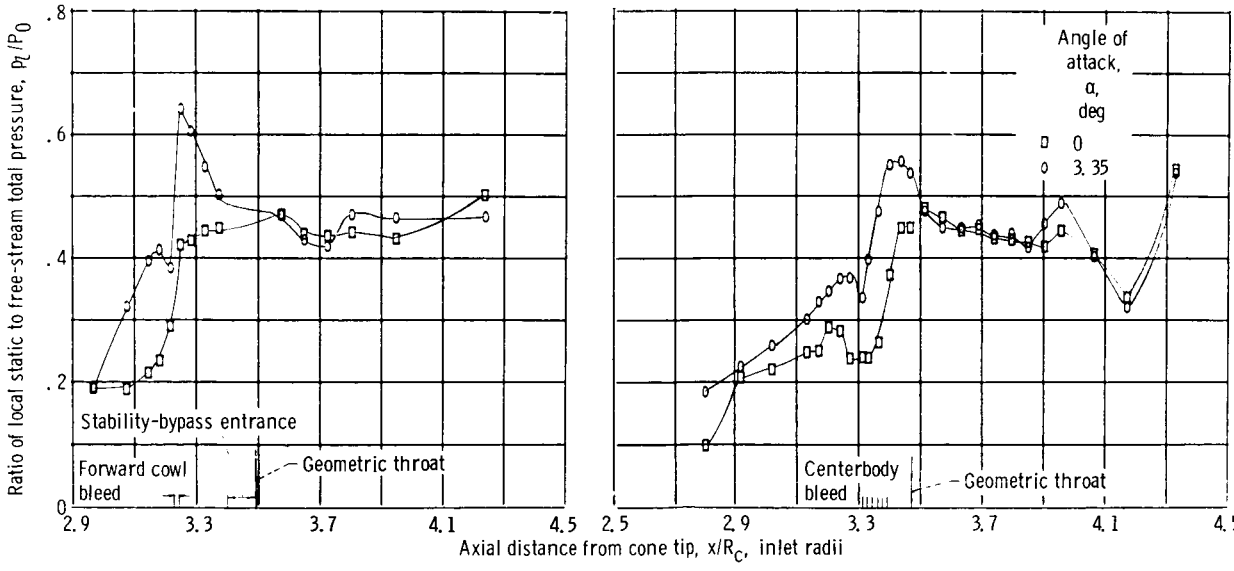

(a) Internal cowl surface pressure distributions.

(b) Centerbody surface pressure distributions.

Figure 21. - Static-pressure distributions at zero angle of attack and maximum angle of attack before unstart. Configuration SS.